

## Article

# Harvesting Systems for RF Energy: Trends, Challenges, Techniques, and Tradeoffs

Surajo Muhammad <sup>1</sup>, Jun Jiat Tiang <sup>1</sup>, Sew Kin Wong <sup>1</sup>, Ali H. Rambe <sup>2</sup>, Ismahayati Adam <sup>3</sup>, Amor Smida <sup>4,\*</sup>, Mohamed Ibrahim Waly <sup>4</sup>, Amjad Iqbal <sup>5,\*</sup>, Adamu Saidu Abubakar <sup>6</sup> and Mohd Najib Mohd Yasin <sup>3,7,\*</sup>

- <sup>1</sup> Centre For Wireless Technology (CWT), Faculty of Engineering, Multimedia University, Cyberjaya 63100, Selangor, Malaysia; doguwa\_2002@yahoo.com (S.M.); jjtiang@mmu.edu.my (J.J.T.); skwong@mmu.edu.my (S.K.W.)
- <sup>2</sup> Department of Electrical Engineering, Universitas Sumatera Utara, Medan 20155, Indonesia; ali3@usu.ac.id
- <sup>3</sup> Advanced Communication Engineering (ACE) Centre of Excellence, Universiti Malaysia Perlis (UniMAP), Arau 02600, Perlis, Malaysia; ismahayati@unimap.edu.my
- <sup>4</sup> Department of Medical Equipment Technology, College of Applied Medical Sciences, Majmaah University, Al-Majmaah 11952, Saudi Arabia; m.waly@mu.edu.sa
- <sup>5</sup> Institut National de la Recherche Scientifique (INRS), Montréal, QC H5A 1K6, Canada
- <sup>6</sup> Department of Electrical Engineering, Ahmadu Bello University, Zaria 810211, Nigeria; adams4real56@gmail.com
- <sup>7</sup> Faculty of Electronic Engineering Technology, Universiti Malaysia Perlis (UniMAP), Arau 02600, Perlis, Malaysia
- \* Correspondence: a.smida@mu.edu.sa (A.S.); amjad.iqbal@inrs.ca (A.I.); najibyasin@unimap.edu.my (M.N.M.Y.); Tel.: +234-7039698189 (A.I.)



**Citation:** Muhammad, S.; Tiang, J.J.; Wong, S.K.; Rambe, A.H.; Adam, I.; Smida, A.; Waly, M.I.; Iqbal, A.; Abubakar, A.S.; Mohd Yasin, M.N. Harvesting Systems for RF Energy: Trends, Challenges, Techniques, and Tradeoffs. *Electronics* **2022**, *11*, 959. <https://doi.org/10.3390/electronics11060959>

Academic Editors: Costas Psychalinos and Inhee Lee

Received: 10 February 2022

Accepted: 14 March 2022

Published: 20 March 2022

**Publisher's Note:** MDPI stays neutral with regard to jurisdictional claims in published maps and institutional affiliations.



**Copyright:** © 2022 by the authors. Licensee MDPI, Basel, Switzerland. This article is an open access article distributed under the terms and conditions of the Creative Commons Attribution (CC BY) license (<https://creativecommons.org/licenses/by/4.0/>).

**Abstract:** The RFEH design challenges can be broadly classified into overall radio frequency direct current (RF-to-DC) power conversion efficiency (PCE), form factor, operational bandwidth (BW), and compactness. A detailed overview of the essential components of an RFEH system is presented in this paper. Various design approaches have been proposed for the realization of compact RFEH circuits that contribute immensely to mm-wave rectenna design. Effective mechanisms for configuring the rectenna modules based on the recommended spectrums for the RFEH system were also outlined. This study featured a conceptual viewpoint on design tradeoffs, which were accompanied by profound EH solutions perspectives for wireless power communications. The work covers some challenges attributed to 5G EH in mm-wave rectenna: from a controlled source of communication signals to distributed ambient EH and system level design. Conversely, the primary targets of this work are to: (I) examine a wide range of ambient RF sources and their performance with various antennae and RF-rectifier layouts; (II) propose unique rectenna design techniques suitable for current trends in wireless technology; (III) explore numerous approaches for enhancing the rectenna or RF-rectifier efficiency in a low-power ambient environment; and (IV) present the findings of a comprehensive review of the exemplary research that has been investigated. These are aimed toward addressing the autonomous system's energy challenges. Therefore, with the careful management of the reported designs, the rectenna systems described in this study would influence the upcoming advancement of the low-power RFEH module.

**Keywords:** RF energy harvesting (RFEH); impedance matching network (IMN); rectification unit; power conversion efficiency (PCE); rectenna; RF-rectifiers; source antennas

## 1. Introduction

The exponential advancement of wireless communication technology (WCT) and ultra-low-power devices draws the attention of researchers daily. Technological inventions and innovations in the fields of the IoT [1–4], autonomous driving [5], biomedical implantable devices [6], industrial IoT [7], wireless sensor network (WSN) [4,8], and many more are

the sources of various applications drivers. There is a need for miniaturized and high-precision power sources as the dimensions of modern semiconductors are scaled down to millimeters (mm) and sub-mm [9,10]. Recently, the RFEH module for extracting RF energy in the mm-wave spectrum have not been established because of the lack of widespread deployment of mm-wave networks [11]. The concept of RFEH and wireless power transfer (WPT) in mm-wave are emerging techniques in wireless power communications [11,12]. This is attributed to the 1990s breakthrough in the mm-wave power transmission and rapid development in mm-wave 5G architecture [10,11].

Meanwhile, we are becoming heavily reliant on electricity to accomplish most of the daily routine activities. The trend in technological advancement considers energy to be one of the leading challenges related to most of the device's operations because of the energy recursion [13]. On 30 April 2015, Anders S. G. Andrae and Tomas Edler from Huawei Technologies Sweden AB published an article "On Global Electricity Usage of Communication Technology: Trends to 2030" [14]. He explained and projected the global electricity consumption attributed to communication technology (CT) by 2030 among data centers, consumer-end devices, and communication networks. One of the key issues raised is that by 2030, the CTs can exploit over 51% of the global electricity consumption. An important finding posed by this work was the need to look into other sources of sustainable energy. Hence, contributions from modern (EH) technology can significantly ease the demand for energy-dependent equipment (such as power cords, power accessories, and battery cells) in the future. Applying the concept of green energy to supplement the conventional power generation system will substantially reduce the environmental pollution.

Many researchers have studied EH systems, which involve the process of energy transformation from various forms to electric energy, during the last few decades [15–18]. A variety of technologies have been developed to harness sustainable energy from different sources [19–23]. Among a few forms of the EH, sources comprise hydro, wind, solar, biomass, acoustic, RF, etc. [19,24]. Hydro, solar, and wind energies are among the commercialized EH sources because of their capability to handle large volumes of energy from the surroundings through hydro and wind turbines, solar panels, etc. [18,25,26]. Hence, the performance of hydro, solar, and wind EH sources depends heavily on the specific natural operational conditions and requirements such as location, time, and weather [17,27–29].

Recently, the exponential growth of wireless technology attracts the researchers' attention toward RFEH from the ambient EM wave radiating in space [30–35]. Over the years, the power density of ambient EM signals is expanding because of development in mobile cellular networks, TV-based entertainment, and Wi-Fi-enabled applications, which pave the way for RF-powered applications [36–39].

The power requirements of small electronic devices and their future application drivers are highlighted in Figure 1 [40]. The intercepted energy signal from the RF sources was revealed to have a minimal power density that spans from 0.001 to 0.1  $\mu\text{W}/\text{cm}^2$ . For the time being, proper management of the harvested energy can be deployed for low-power devices and sensors nodes with minimal energy consumption [41–44].

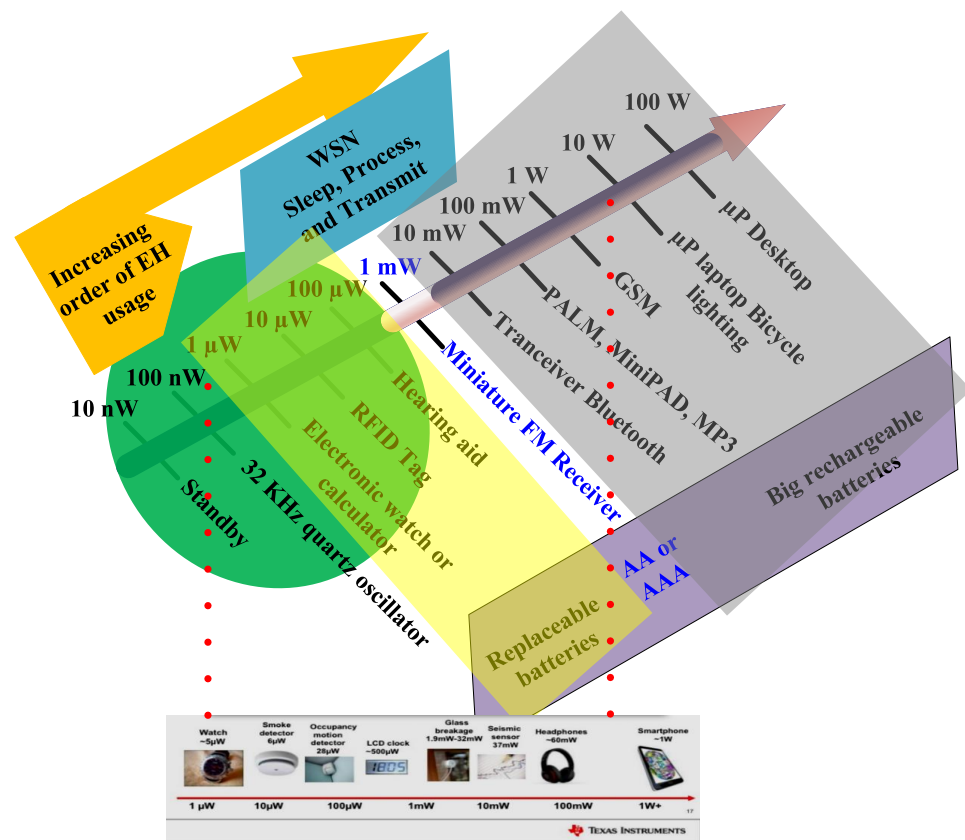


Figure 1. The power requirements of small electronic devices and their future applications [40,45,46].

An antenna combined with an RF-rectifier is responsible for harvesting the available ambient EM signals [47–49]. Integrating the antenna with the RF-rectifier is termed a rectifying antenna, which is also known as a rectenna [50,51]. The antenna picks up the radiated EM waves from the surroundings, which are then transformed into usable DC signals through the RF-rectifier [15,52]. An antenna-less rectenna is classified as an RF-rectifier [13]. The RF-rectifier comprises a rectifying diode, a DC-pass filter (storage element), and  $R_L$  match by an IMN [30,36,52–55]. The main components of the RFEH system are given in Figure 2. A good IMN ensures maximum transfer of the received RF signals from the antenna, which are then transformed into DC source by the rectifying diode. The DC-pass filter is introduced to eliminate higher-order harmonics from entering the  $R_L$  [56–59]. The performance of the output impedance and the output DC supply is handled by the DC-pass capacitor filter [36,60].

Various sources of EM waves exist at different operating frequencies scattered in multiple directions. The EM environment is regarded for extracting RF energy because of the influences from digital broadcast and cellular mobile communication. Ambient RF energy sources are accessible at various operating frequencies and power densities. Thus, the proper selection of RF signal sources is critical when targeting an RF harvester that can be deployed for powering a module of an autonomous system [61,62]. To ensure and identify a proper RF signals for harvesting, it is important to evaluate essential factors of the radiating signal. These parameters comprise frequency,  $P_{in}$ , location, coverage area, and the transceiver base station (BS) [63–66]. Many RF EM sources, such as GSM BS transceivers, Wi-Fi networks, WiMax networks, 5G networks, Medium Wave (MW) broadcast stations, and so on, are nowadays available in semi-urban and urban environments [67,68]. The new and evolving technological innovations have resulted in recent

WCT advancements. The growing demand for such inventions resulted in one or more application drivers on the IoT, industrial IoT, autonomous driving, smart farming, smart cities, wearable devices, and many other areas. Hence, in densely populated areas, we can monitor and identify thousands, if not millions, of devices in one location.

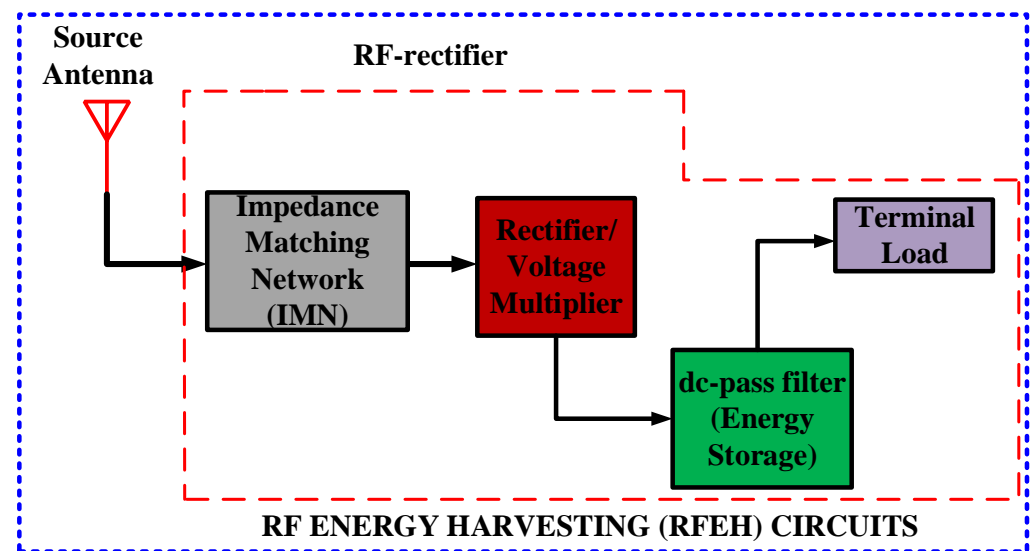


Figure 2. Block diagram of the basic RFEH system [52].

## 2. Significance of the Research

A number of researchers have been making efforts toward the enhancement of battery efficiency [69–72]. Thus, the key requirements of autonomous systems are at odds with the constraints imposed by the battery drawbacks, such as short lifetime, the need for frequent recharging or replacement, and the release of various toxic chemicals [73–75]. Hence, the ambient RFEH system is an emerging technology that allows low-power devices to operate for extended periods, making it a viable alternative to the traditional battery source [76–78].

EH via microwave beams has been previously deployed to handle a variety of autonomous systems. Techniques such as unmanned aerial vehicle (UAV) [79] and solar power satellite (SPS) [80] are presented for high-power wireless applications. This technology has recently become commercially available with the rapid development of devices with low power requirements. Radio frequency identification (RFID) is an example of how this method is successfully employed [45,81–83]. The applications require an EM energy source that can be appropriately managed for the successful operations of the RF harvester. The number of wireless communication devices such as wearable devices, WSN, and implantable devices, which have been deployed for the past few decades, has proliferated [84–91]. Such growth in wireless applications necessitates the development of additional sources of energy. Consequently, the low power requirements in today's autonomous systems have opened the door for the use of ambient RF energy modules as an alternative source of energy [44,92–94]. The power density of the available EM waves is statistically steady regardless of climate conditions. This is one distinct feature of the RFEH system because of the transmission of EM waves over multi-path fades propagation channels. The significance of the RFEH harvesters can be outlined as follows:

### Wireless Power Transfer (WPT)

- The recent development in low-powered RF devices makes the RFEH system a suitable source of energy compared to their wired counterpart, which serves as an additional source of energy;

#### Economical value

- A simple RFEH module integrable with other boards can be deployed in remote areas to replace batteries, which in turn reduces the maintenance costs;

#### Longer operational life of device and health monitoring

- Provides long-lasting operation to a device(s) (that can be deployed in body area network (BAN) applications). For example, it is necessary to have a high uptime power supply for medical conditions such as prostheses, cardiac pacemakers, and it is not highly recommended to use batteries or any form of a traditional source of power;

#### Security surveillance

- For example, it is challenging to access the power source for maintenance, and there is no connected power supply accessible as found in wild forest fire detection, earthquake-prone locations, etc.

#### RF-to-DC Power Conversion Efficiency (PCE)

A typical method of RF-to-DC PCE enhancement in the RFEH system is the connection of the diode to the load  $R_L$  via the source antenna. To harvest a significant portion of the incoming RF signals from the antenna source, a rectifier circuitry with high PCE is required. Variables such as  $P_{in}$ , diode selection, junction capacitance, operating frequency(ies), higher-order harmonics, and  $R_L$  are known to be the major efficiency influencers. A diode that performs well at relatively high  $P_{in}$  levels does not have the same attributes when operating at a low power level, such as  $-20$  dBm. The rectification unit deployed in the RF-rectifier circuitry is mostly a combination of resistive and capacitive elements.

The ratio of the output DC power ( $P_{dc}$ ) to the  $P_{in}$  in an EH system is referred to as RF-to-DC PCE [30,52,95]. The ability of the RF-rectifier to transform the received RF signals into viable output DC signals is given by Equation (1). This is achieved when the output impedance of the antenna and that of the load impedance ( $Z_L$ ) become conjugate to each other through proper impedance matching. This ensures a maximum transfer of power from the antenna source to the rectification section [52,96]. The authors in [97] demonstrated the process of RF-to-DC PCE operation in RFEH circuits. Two major findings were illustrated from the authors. Firstly, the RF-to-DC PCE is a factor of employed circuit elements, and the lesser the components, the better the performance of the harvester and vice versa [4,15]. This is due to the minimum  $P_{in}$  requirement of the rectification section. Therefore, a rectifying diode with a low turn-on voltage is needed based on a single or voltage multiplier topology to facilitate the efficient operation of the RFEH system. The higher the number of diode or the multiplier stages, the higher the voltage at the expense of minimal load current. Whereas the reduced number of diode or multiplier stages offers quick and efficient charging, with a considerable decrease in the  $V_{dc}$  across the load. As such, a tradeoff has to be made between the number of stages and that of the circuit performance in the design of the RFEH system [92,98–100]. Secondly, the RF-to-DC is determined by the amount of power available at the input of the RF-rectifier. The RF-to-DC PCE increases in lockstep with the  $P_{in}$ , reaching a peak value shortly as the amplitude of the rectifying diode approaches the diode breakdown voltage ( $V_{br}$ ) [28,36,101]. Hence, the diode reverse current becomes large, which in turn decreases the overall RF-to-DC PCE. In addition, the impedance of a diode is affected by its aspect ratio and the number of stages. Thus, the higher  $R_L$  can result in a larger  $V_{dc}$ . This does not rule out the possibility of achieving peak power with a smaller  $R_L$ . As a result of this power dependency, the RFEH design must be tuned and optimized to achieve the desired goal at a given power level.

$$\eta_{PCE}\% = \frac{P_{dc}}{P_{in}} \times 100\% = \left(\frac{V_{dc}^2}{R_L}\right) \times \left(\frac{1}{P_{in}}\right) \times 100\% \quad (1)$$

where  $\eta_{PCE}$  is the RF-to-DC PCE,  $P_{dc}$  is DC output power across the load  $R_L$ , and  $V_{dc}$  gives the output DC voltage.

### 3. RF Spectral Survey

To determine the potential of implementing an RF harvester in an area, the levels of the radiated RF power signals must be determined, because these will identify and deduce the type of RF harvester's features and specifications to be deployed in a location. This work determines the levels of the received RF ambient power available in the Multimedia University (MMU), Cyberjaya campus as a basis for designing efficient RFEH components in a given location.

#### 3.1. Site Surveys for Ambient RFEH

Next, we need to discover the available received ambient power levels in the MMU. The campus is designated for surveying RF energy because it is considered to be in a semi-urban environment. The RF spectral survey is carried out between the frequency span of 0.500 to 3.00 GHz on the RF spectrum analyzer. This spectrum is placed under the ultra-high-frequency or microwave spectrum. A TTI PSA6005 spectrum analyzer measures the available received ambient RF power. Table 1 provides the specifications of the equipment for the RF spectral survey. A commercial whip antenna from ABRACON is used for the setup connection. The antenna operates from 0.700 to 2.700 GHz, with a peak gain of 5 dBi [102]. The proposed antenna-measured realized gain across the respective operating band is presented in Table 2. All the measurements of the available received RF ambient power are conducted in the daytime between the range of 8:00 a.m. and 6:00 p.m. The 6 GHz spectrum analyzer was calibrated to measure the received signal strength in the frequency range of 0.50 to 3.00 GHz of the microwave spectrum. For every sample point recorded, about 90 s were assigned to ensure better measurement of the received RF power. The RF spectrum analyzer setting guarantees that intercepted power levels from non-dedicated RF sources in the semi-urban surrounding are measured and reported accordingly.

**Table 1.** RF spectral survey device specifications.

Device Name	Model	Main Feature Characteristics
Spectrum Analyzer	Aim TTI PSA6005	Portable, BW: [3 kHz to 6 GHz], Resolution BW: 1 kHz
Whip Antenna	ABRACON AEACAD097015-S698	BW: [0.7 to 2.7 GHz], Peak Realized Gain: 5 dBi, Maximum Efficiency: 67%, Mountable.

BW: operating bandwidth.

#### 3.2. Selection of Available Frequency Bands

A 6 GHz spectrum analyzer is deployed to determine the level of the available RF ambient power in the terrain. During the measurement process, each of the strategic locations is demarcated within 90 to 190 m across a straight-line path. Three sample points were recorded for each straight-line path at an interval of 30 m. Following the 190 m straight-line measurement, a 90° interval was set for each of the study locations to undertake comparable data collection (i.e., four different sectors per study location). Therefore, the measurement is repeated across each strategic location, as shown in Figure 3 [76,103]. During the RF survey process, over 20 study locations were established. The survey process was conducted during the project's early stage for seven months, from June 2019 to December 2019.

The precise frequencies for each band are determined by the Malaysian communications and multimedia commission (MCMC) licensed frequency band allotment. The frequency spectral bands for operations by various telecommunications operators, such as TV stations, GSM-900, GSM-1800, 3G/UMTS-2100, Wi-Fi, LTE-2600, WiMax, and many

more, were categorized and allocated. The received ambient RF power from the telecommunication operators in the country was recorded by the spectrum analyzer. A significant level of the received RF power level was observed across the five major operating bands comprising GSM/900, GSM/1800, UMTS/2100, Wi-Fi/2.4/2.45, and LTE/2600. Hence, Figure 4 shows the reported ambient RF power levels for the accessible frequency bands.

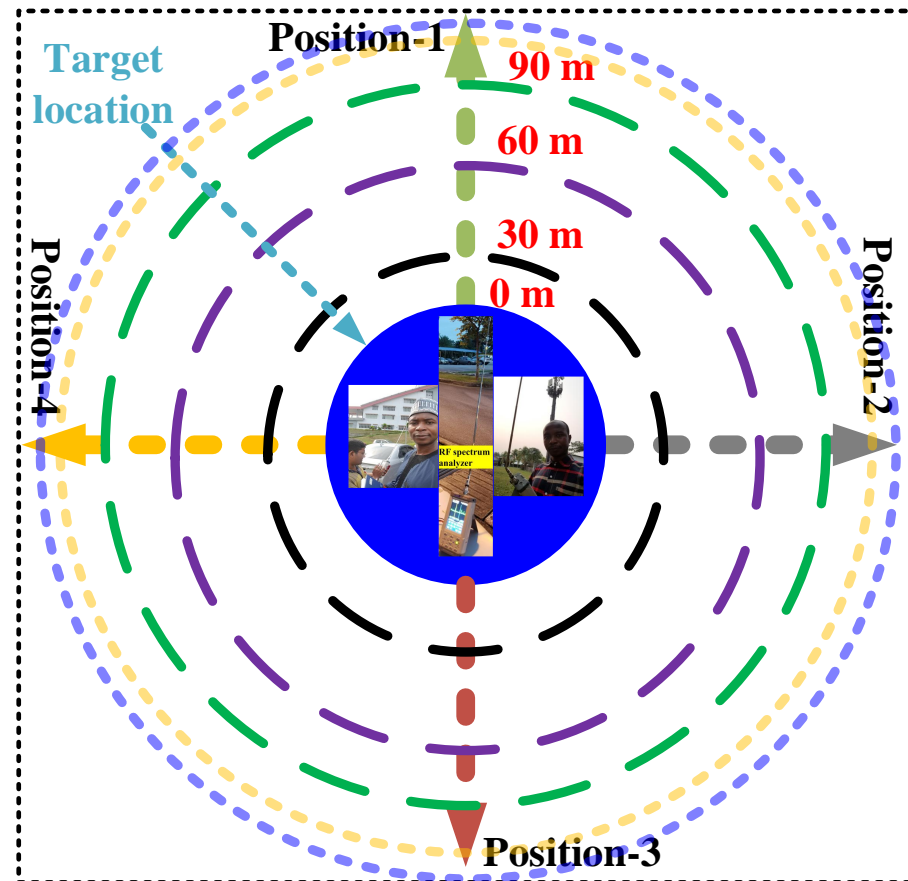


**Figure 3.** Strategic demarcation of the RF spectral survey at Multimedia University, Cyberjaya campus.

Each sample point interval is recorded, and the average result is calculated for each span along a straight-line path. The four sectors were all subjected to a similar computation. This task was repeated for all the measured data. Table 2 summarizes the received ambient RF power and its corresponding averages for the five major operating bands in the institution. It can be observed from Table 2 that the intercepted power levels at the BS are one or two orders of magnitude higher than the mobile power levels across the GSM/900, GSM/1800, and UMTS/2100, and Wi-Fi/2.45 spectrum. These four frequency bands recorded the highest average power of  $-21.2$ ,  $-15.3$ ,  $-22.5$ , and  $-17.7$  dBm, respectively. In addition, the capability of the LTE/2600 frequency at  $-23.8$  dBm makes it another suitable candidate for the RF harvesting. As a result, the deployment of the RF harvester in a strategic area around BSs is preferable for better performance. Therefore, the potential of these five operating bands becomes the prime focus of the RF harvester design in this work.

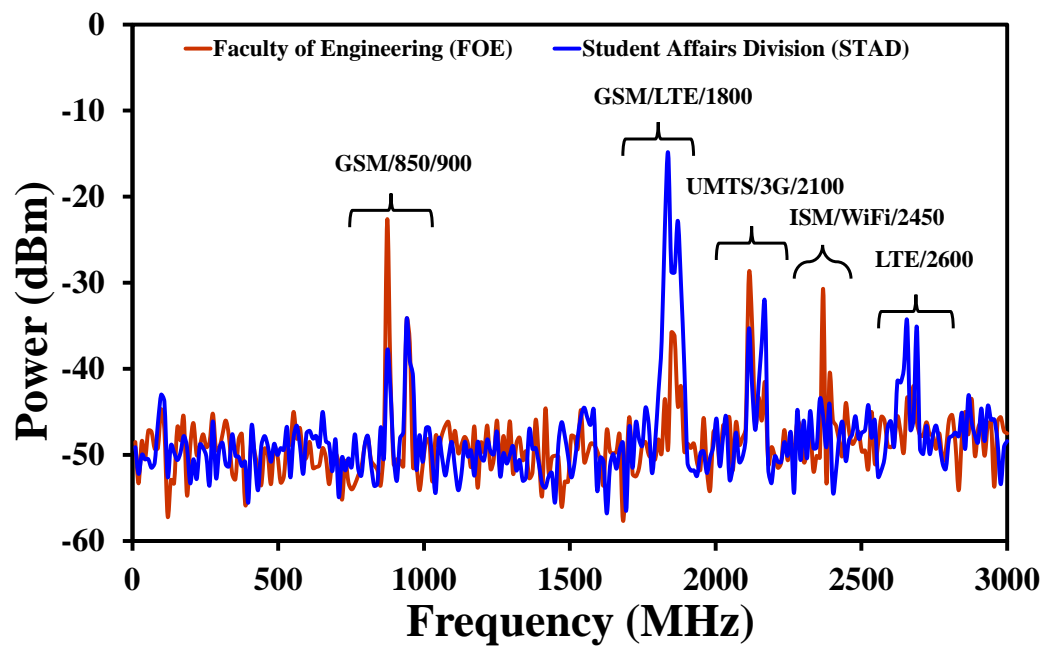


**Figure 4.** Measured received ambient RF power levels at different locations at Multimedia University, Cyberjaya Campus [76].

**Table 2.** Received ambient power from various public telecommunication bands.

Band	Operating Frequency (GHz)	Received Power Level * (dBm)	Average Received Power (dBm)	Realized Gain [102] (dBi)
GSM900 ( $M_{TX}$ )	0.88–0.915	−45–−26.5	−27.8	4.87
GSM900 ( $B_{TX}$ )	0.925–0.960	−40–−17.5	−21.2	2.56
GSM1800 ( $M_{TX}$ )	1.710–1.785	−47–−40	−42.7	2.85
GSM1800 ( $B_{TX}$ )	1.805–1.880	−35–−14	−15.3	2.92
3G ( $M_{TX}$ )	1.920–1.980	−44–−25.5	−26.7	1.81
3G ( $B_{TX}$ )	2.110–2.170	−43–−20.1	−22.5	2.46
ISM2400	2.305–2.400	−45–−29.7	−30.1	--
Wi-Fi2450	2.400–2.500	−35–−15	−17.7	--
LTE2600	2500–2690	−45–−19.5	−23.8	2.66

\*, The site is located within range of 10 to 190 m. Each sample point is diagonally recorded at an interval of 30 m and 1.8 m high from the close-by cell tower BS. The measurement is repeated at four different locations of the BS (90° apart).

#### 4. RFEH Rectenna

The received RF signal is managed and processed under the specified RFEH approach to activate low-power devices. The accessible RF power density from various sources varies from 0.18 to 84 nW/cm<sup>2</sup> in the ambience environment, which can reach up to 1000 μW/cm<sup>2</sup> from the RF dedicated source [61,63,65,104]. The rectenna has attracted a lot of interest from scholars in recent years, as depicted in Figure 2. Hence, the working principle of the rectenna system stays the same regardless of the application. Figure 5 demonstrates a flow diagram of the basic rectenna system's components, blocks, and applications. Various research studies have been conducted over the years to show the potential of RFEH modules as an additional source of sustainable energy.

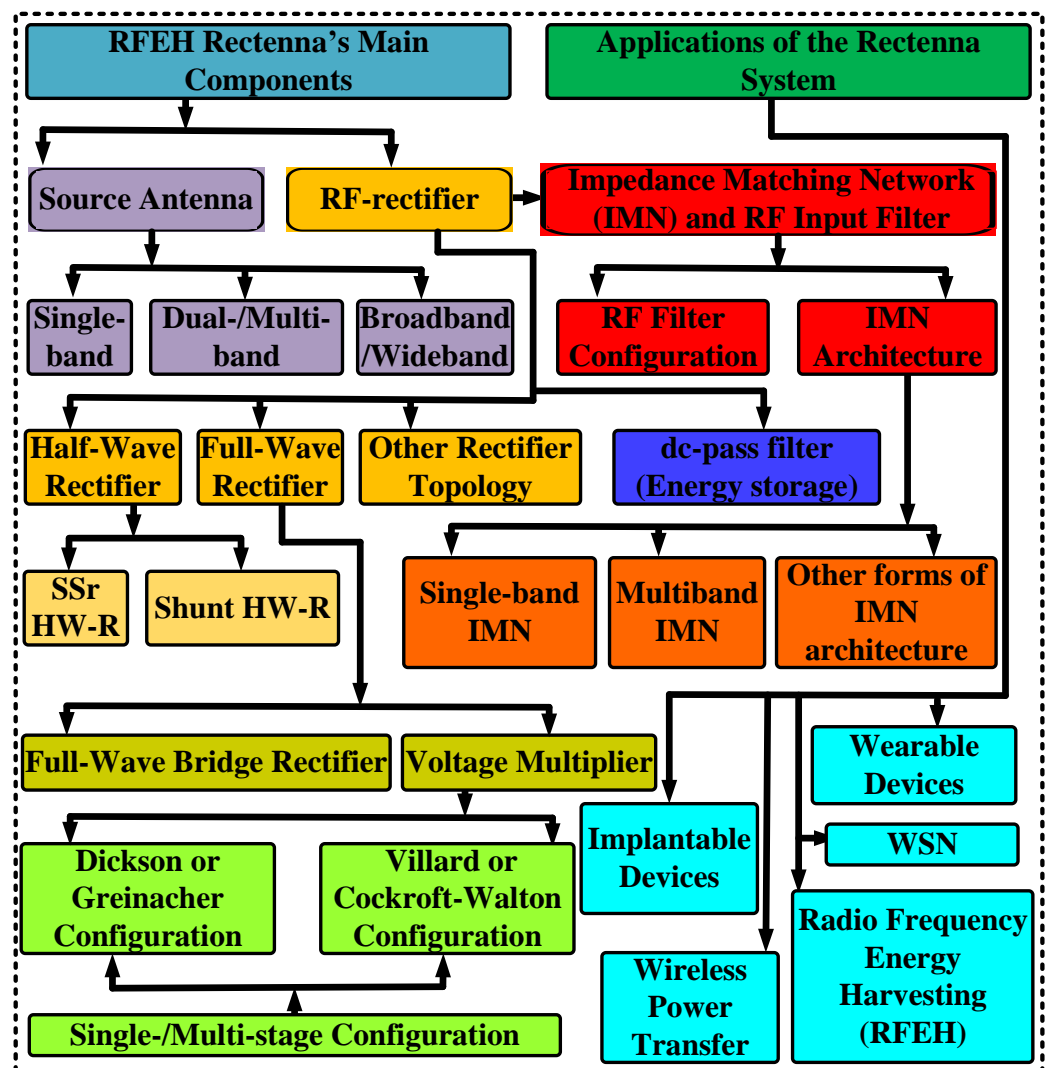


Figure 5. A flow diagram showing several components of the rectenna system [100].

4.1. Antenna for RFEH

An antenna is a type of transducer that transforms EM waves into AC or the other way around [105,106]. It can also be regarded as a transitional structure connecting free space and a guiding device or a TL. Antennas are basically categorized into two:

A transmitting antenna: that conveys the outgoing AC signals into communicable EM waves, and

A receiving antenna: that collects the radiated EM waves and converts them to equivalent AC power for circuit applications [107,108].

Antennas are configured and tuned to function at a specific operating frequency(ies) range while rejecting signals from non-specified bands. Hence, an antenna is regarded as a transceiver device that can be deployed at the transmitting or receiving ends [107,108]. An antenna can be portrayed based on the Thevenin TL model. Equation (2) describes the whole antenna segment using the same TL model.  $R_{L1}$  denotes dielectric and conduction losses that are established alongside the structure of the antenna.  $R_r$  gives the radiation resistance that also determines the antenna radiation efficiency.  $X_A$  provides the imaginary components of the antenna impedance [107].  $V_s$  is the antenna equivalent voltage.  $R_{ant}$  represents the antenna radiation resistance, and input impedance ( $Z_{in}$ ) is from the rectifier or other equivalent circuits [109].

The receiving source antenna is among the most vital segments of the RFEH system's front end. First, the source antenna receives the incoming RF signals, which are then processed and transformed by the RF-rectifier into a DC source in the concurrent stages. The performance of the RFEH source antenna influences the dimension and the complexity of the rectenna circuitry. A wider operation BW, omnidirectional pattern, high gain, compact size, and low profile are among the significant features to be considered in the RFEH antenna's design. Hence, the antenna reactive power source  $V_s$  is modeled using the equivalent wave in Equation (3) [110–113]. For clarity, this section is further divided into three subsections depending on the antenna operating frequency as: (I) Single-band, (II) Dual-band/Multiband, and (III) Broadband/Wideband. Hence, the performances of various RFEH antenna designs that have been reported in the literature are explored in this section.

$$Z_A = (R_{L1} + R_r) + jX_A \quad (2)$$

$$V_s = V_{smax} \sin \omega t \quad (3)$$

where  $V_{smax}$  represents the amplitude of the RF power source passing through the MN at an angular operating frequency of  $\omega$ .

#### 4.1.1. Single-Band Antennae

Single-band antennae that are deployed in RFEH rectennas are normally achieved with a narrow operating BW. Various antenna parameters are taken into account during a single-band antenna design process from a performance perspective [114,115]. An antenna's gain is an essential parameter. An RFEH source antenna with a high gain can capture more signals from the environment, because the antenna's gain is proportional to its electrical aperture. Antennae with a high gain are needed when the direction of incidence of the incoming RF signal is predictable [116–122]. In addition to high antenna gain, the antenna's omnidirectional pattern ensures better reception of incoming RF signals, especially in an ambient environment. Thus, an RFEH antenna with high gain characteristics is important in order to have a maximum reception of the incoming energy and improve the RF harvester PCE with a better  $V_{dc}$ .

The authors in [123] presented a single-band antenna operating at 2.450 GHz. This design achieved a gain of 1.250 dBi through an aperture coupling slot with an isosceles triangular shape. A 2.450 GHz antenna is described by the authors in [124]. The antenna is realized by adding a U-slot and trimmed corners to the radiator, which offers a 1.480 dB AR. The authors in [125] incorporate a dual-fed antenna using two slot lines with transversal ends. This array of CPW source antennas operates at 5.800 GHz. A back-feeding concept is employed in this work to augment the BW of the antenna. The design realized an AR of 0.680 and a gain of 6.300 dBi. The authors in [126] reported an antenna design approach by inserting an air gap into a layered dielectric resonator antenna (DRA). This design recorded gain and BW enhancement across the 5.800 GHz  $f_0$ . In addition, the authors in [127] reported that adding an aluminum core with metallic Vias into a layered DRA architecture improves the gain and the operation BW of the RFEH antenna.

The authors in [128] make use of the differential feeding mechanisms to improve the gain of the antenna, operating at 2.450 GHz. The need for a BALUN is avoided through the differential feeding approach. The antenna occupies a size of 100 mm × 70 mm on the PCB and achieved a peak gain of 5.470 dBi from the design approach. Additionally, the differential feeding reduced higher-order harmonic modes. To obtain an appropriate gain in a differential feeding scenario, the ports that fed the source antenna must be configured correctly. An array of antennas in a single-band rectenna is also studied for improving antenna gain. The authors in [129] reported an array of antennas that is realized with the help of a dual-rhombic loop antenna, operating at 5.800 GHz. The authors in [130] investigate a unique antenna design using an aperture coupling to achieve a patch array structure. The gain improvement of the aperture-linked antenna array facilitates the enhancement of the incoming RF signals above 1 mW. The frequency of operation for this

antenna is 5.800 GHz. The design of an antenna array for GSM-900 is reported by the authors in [131]. Two T-shape monopole antennae make up this antenna array. The array designed improves antenna gain. The compactness of this array structure is maintained by integrating stubs into the bottom ground. The authors in [132] demonstrated a directional multi-port-pixel antenna technique for RFEH systems. This design is realized using a grid of antenna arrays connected at four different port terminals. The overall antenna structure has a dimension of 100 mm × 100 mm. This antenna operates at a frequency of 1.800 GHz and achieves a gain of 5.500 dBi. The approaches recently demonstrated in the literature toward the enhancement of the RFEH antenna gain have also introduced circuit complexity, besides increasing the overall antenna electrical length. Furthermore, it is observed that the antenna array is characterized by a narrow operational BW, which in turn limits the harvesting capability of the RFEH antenna. As a result, many approaches are further explored to accomplish antenna miniaturization.

The authors in [133] presented a way of compacting the antenna by folding the radiating elements. The antenna operates at 0.900 GHz with a dimension of 62 mm × 62 mm. A circular-shaped is deployed to achieve antenna compactness by the authors in [134]. The geometry of this design is realized by widening the circular fold curves. This antenna operates at a frequency of 2.450 GHz. The work also realized an operational BW of 150 MHz from 2.350 to 2.500 GHz. The concept of the spiral planar inverted-F antenna (SPIFA) is reported by the authors in [85]. To demonstrate compactness, a shorting pin is situated on top of the radiator plate's corner. This ensures the source antenna resonates at a frequency below quarter-wavelength. This antenna operates at 673.000 MHz and achieved an AR of less than 3 dB. However, several of these presented approaches are subject to either a feeding port modification at a suitable location or to a large antenna size due to array elements. Therefore, a significant quantity of power is provided for the single-band antenna layout using either a large dimension of a radiating element or a high antenna gain. However, an antenna array normally comes with a wide aperture dimension. This extends the size of the antenna and therefore the rectenna's size. Therefore, the use of a source antenna with a reasonable gain is very important in the design of the RFEH system.

#### 4.1.2. Dual Band and Multi-Band Antennae

The multi-band antenna extends a wide range of required  $f_0$  for harvesting the incoming RF signals. Therefore, the antenna captures more available energy from the surroundings. Some of the available literature reported for the design of the RFEH multi-band antennas is discussed in this section. The authors in [135] demonstrated the design of a triple-band RFEH planar inverted-F antenna (PIFA). The triple-band functionality is realized by adding an meandered line (MDL) structure into the design. This antenna operates at a frequency of 402, 433 MHz, and 2.450 GHz. This design realized a quite low-peak antenna gain of  $-7$ ,  $-11$ , and  $-15$  dBi across the three operating frequencies, respectively. A dual-band RFEH antenna is implemented by the authors in [94]. The antenna is realized by integrating the rectangular radiator with a folded dipole. This antenna resonates at 0.915 and 2.450 GHz. The authors in [136] reported that the deployment of multi-band characteristics in the rectifier design offers a better performance as compared to a single-band or dual-band counterpart. For attaining a broader operational BW with an improved gain, a pentagon-shaped DRA is reported by the authors in [137]. This design is achieved by integrating a PDRA with a narrow-notch rectangular slot. This antenna resonates at 0.900 and 1.900 GHz. With the introduction of an expensive DRA into the design, the source antenna recorded a peak gain of 6.800 dBi. The authors in [138] discussed the design of a dual-band antenna. The antenna is realized through a two-arm structure. A long fractal structure arm produces a lower  $f_0$  at 0.870 GHz, whereas a shorter one generates a higher operating band at 1.830 GHz. The antenna realized a peak gain of 0.950 and 3.150 dBi across the two operating frequencies. A two-port triple-band RFEH antenna configured with an L-probe was developed by the authors in [139]. The L-probes of the antenna are connected back-to-back. This design operates at 0.9250, 1.850, and 2.150 GHz, with an

overall dimension of 17.5 cm × 20 cm. The concept of loaded slots to generate an antenna with multi-band capabilities is further investigated. Antenna design techniques, such as an array [41,140–142], air gap [143], differential feeding [144,145], and aperture-coupled feeding technique [146,147], are some approaches used. Either large antenna electrical size or circuit complexity hampered these design approaches. One of the important factors in the design of multi-band antennae is good impedance matching in order to maximize the reception of the RF signal through high gain. Multi-band antennae with reasonable footprints are desirable for a variety of rectenna applications.

#### 4.1.3. Wideband and Broadband Antennae

Broadband antennas are typically implemented across a wide frequency range. Hence, the RFEH antenna can pick up the available RF signal from various sources because of the wide frequency coverage. Wideband and broadband antennae have been the subject of several pieces of literature, which are also discussed in this section. The authors in [148] presented a unique broadband slot antenna. The RFEH antenna is realized through the use of a grounded CPW to enhance impedance matching. The antenna occupies a total dimension of 135 mm × 93 mm and operates between 2.000 and 2.700 GHz with an FBW of 28.6%. The use of a slotted or a defected ground structure (DGS) is exploited to achieve broader operational BW [149–156]. A broadband RFEH antenna is reported by the authors in [149]. The operational BW and gain of the RFEH antenna are improved by coupling the ground plane with a DRA, and a rectangular-slit is also added to the underneath slot. The source antenna operates between 1.670 and 6.700 GHz with a gain that ranges from 2.200 to 8.700 dBi. In addition to the deployment of the DRA, a metallic reflector plays a role in the significant improvement of the antenna gain, with a total dimension of 100 mm × 110 mm × 31.7 mm. The authors in [150] developed a wideband antenna operating between 0.890 and 5.500 GHz. The antenna is realized by coupling a circular radiator with a DGS that also incorporates another rectangular slot on the upper layer. The antenna attains a peak gain of 4.3 dBi and occupies a size of 100 mm × 120 mm. The authors in [157] investigate the use of a fractal approach on the CPW RFEH antennas. The antenna is realized through two rotating equilateral triangular slots to achieve the fractal structure. This design covers an operational BW of 0.880 to 8.450 GHz. The authors in [158] described a CPW broadband antenna for RFEH application. The antenna is designed by adding a pair of cross rectangular intersection slots into the radiating element. The antenna covers a range of 5.500 to 6.700 GHz with a peak gain of 8.56 dBi, with an FBW of 20.68%. The authors in [159] demonstrated the concept of a log periodic dipole (LPDA) RFEH antenna. The antenna is constructed with 20 LPDA elements and covers the range of 0.570 to 2.750 GHz. The authors in [160] described a unique slotted wideband antenna design for the RFEH system. The source antenna is designed by embedding the bottom ground with a pair of symmetrical slots on each side of the feed line. Two different slot configurations are integrated into the radiating element of this design to achieve the desired target. The antenna realized an operational BW of 1.100 GHz from 2.000 to 3.100 GHz.

Getting a source antenna and RF-rectifier circuits to properly match in the wideband RFEH system is quite challenging because of the diode nonlinearity. According to the available literature, the deployment of DGS and loaded-slot structures into the ground plane are the most commonly used approaches to achieve wideband operation. Section 4.1.2 presents several antenna design techniques for the RFEH applications that exploit multiple frequency bands. Hence, it is discovered that frequency bands comprising GSM-900, GSM-1800, UMTS-2100, ISM-2400, Wi-Fi/2450, and LTE-2600 are the most exploited spectrum for the RFEH system. Additionally, other operating frequencies such as 3.500 GHz for WiMax and 5.800 GHz for Wi-Fi/5.8 are also being investigated, but they contribute less energy for RFEH [15,75,96,161–168].

#### 4.2. Impedance Matching Network (IMN) for RFEH

One of the most critical segments of microwave components or systems is impedance matching. This is a technique of getting one impedance terminal to appear approximately similar to the impedance of the other corresponding terminal [107,108]. Matching the  $Z_L$  to the source or internal impedance is the most important aspect to consider during the MN design process. Impedance matching is achieved when the characteristic impedance ( $Z_0$ ) of a source terminal is approximately equal to that of the  $Z_L$ . This ensures maximum supply of power from the source to the load. However, to accomplish the optimum transfer of power between the two ends, the MN needs to be lossless, which is impractical. Hence, the RFEH techniques need to ensure an optimum transfer of power between the receiving antenna and the  $R_L$ . The components of the RF-rectifier are modeled and considered looking from the load. The incident wave is reflected at the  $R_L$  because of impedance mismatch, resulting in a decrease in overall circuit performance or RF-to-DC PCE [100,158,169–171]. MN also aids the DC-pass filter to block the higher-order harmonics induced by the rectifying diode that can be re-radiated to the antenna source and cause further loss [172,173]. Therefore, an MN is desirable between the source antenna and the rectification section. Various types of components and circuit elements can be employed in the MN's realization [172–176]. This section will highlight the basic design and importance of the IMN approaches.

##### 4.2.1. Single-Band MN

Impedance matching circuits are implemented using lumped elements, distributed microstrip transmission lines, or a combination of the two techniques. As compared to a distributed network line, an MN circuit based on lumped elements exhibits lower QF, providing an improved BW. However, lumped elements are attributed to additional parasitic capacitance properties, making them undesirable for operating at high frequencies. Hence, the design of an MN for harvesting RF signals over a single frequency band can be easily realized using various MN techniques based on lumped elements or distributed networks, as highlighted by the authors in [15,100,177,178]. Some of the most widely deployed lumped and distributed circuit configurations for IMN comprise a shunt-MN, series-MN, L-section MN (configured as series-shunt or shunt-series),  $\Pi$ -section MN, T-section MN,  $\gamma$ -section MN, and filters (such as LPF, BPF, and BSF) [15,179–181]. The authors in [182] reported a single band RF harvester. This design is realized using a six-stage diode configuration at 0.900 GHz. The design achieved a  $V_{dc}$  between 0.150 and 0.500 mV. The authors in [183] designed a multi-port RF harvester. In the process, three separate RF-rectifiers were interconnected through an external DC combining technique. The RF harvester is designed to operate at 1.840 GHz. Another RFEH circuit designed based on an external DC combiner approach is reported by the authors in [184]. The RF harvester is realized by integrating multiple RF-rectifiers into a sixteen-port antenna. In the design, four RF-rectifiers operating at 0.940 GHz were assigned to four of the antenna ports, and the remaining twelve ports were integrated with the 1.840 GHz RF-rectifiers. As a result of the autonomous characteristics of IoT devices and sensor nodes, the operation of a single-band RF harvester is inefficient [183,185]. In addition, most of the ongoing RFEH research for long range focuses on designing the RF-rectifier using a multi-stage voltage multiplier or an MN with a multiple lumped elements. The use of multiple components to realize EH circuits degrades the overall performance system. Additionally, a compact, planar, and lightweight EH circuit is desirable to provide ease of integration with the current trends of compact devices. Hence, the recent design approach reported by the authors in [41,132,183,184,186–190] did not address the issue of large electrical lengths in the RFEH systems.

Second-order MN circuits give more BW enhancement than the first-order MN circuits for lumped and distributed networks [191]. However, once the order is extended above two, the BW reduces significantly [15,191,192]. An RFEH circuit is presented by the authors in [186]. However, the type of the MN applied is not specified. The design harvests RF signals from GSM-1800 and Wi-Fi/2.45 spectra. The authors in [138] described the

design of a two-band RFEH circuit for harvesting GSM-900 and GSM-1800 RF signals. The input impedance of the two-segment voltage multiplier is matched by a multi-section IMN. Aside from their considerable electrical length, the additional parasitic capacitance reported by the authors in [138,182,186,193–196], reduces the overall circuit’s performance. The authors in [41,183,197] achieved an RF-to-DC PCE enhancement but at the cost of increased electrical size. In addition, introducing an external DC combining technique into the multiple RF-rectifier circuits by the authors in [183,184] adds to the complexity of the overall RF harvester. Hence, the deployment of a multi-band RF harvester is needed. This can also be explained by the random and variable nature of the incoming RF signals. Hence, a severe form of multi-path propagation can cause signal disruption and losses, which can result in nodes or equipment failure [22,183,184].

This paper proposed the design of an L-section MN as one of the frequently employed matching networks for low-power environments using two elements. Additionally, the L-section MN is regarded as a fundamental design stage from which most of the other designs’ configurations can be implemented. The authors in [180,198–200] outline some various IMN configurations. However, it is quite challenging to realize an MN with these flexible attributes for multi-band or wideband operations in the RFEH’s circuit design. The L-section MN can be configured into eight different topologies. During the design process, two different scenarios were investigated to determine the element position of the MN based on a series-shunt or shunt-series topology. A series-shunt topology is normally applied when the source impedance ( $R_s$ ) is less than the  $Z_L$ , whereas a shunt-series topology is typically used when the  $R_s$  is greater than the  $Z_L$ , as depicted in Equation (4).

$$L_{section} = \begin{cases} R_s < Z_L & \text{or } R_s < \frac{1}{G_L} = \text{Series} - \text{shunt}, \\ R_s > Z_L & \text{or } R_s > \frac{1}{G_L} = \text{Shunt} - \text{series}. \end{cases} \quad (4)$$

The circuit’s input impedance of the RF-rectifier is matched to an  $R_s \Omega$  TL using an L-section MN comprising two possible combinations of inductors and capacitors [52,75]. The model comprises an  $jX$  and  $jB$  matching reactance and susceptance across a terminal load with an impedance of  $Z_L$ . The imaginary reactance of the source and the load are canceled and then compared with their respective real part to determine the MN parameters at a given  $f_o$ . Thus, the model equations of the MN are presented through Equations (5)–(10).

The corresponding TL from the  $R_s$  is expressed as:

$$R_s = R_{in} \cdot (1 + Q^2)^{-1} \quad (5)$$

where  $R_{in}$  is the input impedance of the rectification unit in the proposed EH circuit, and  $Q$  provides the quality factor, which is expressed as:

$$Q = \pm \left[ \frac{R_s}{R_{in}} - 1 \right]^{\frac{1}{2}} \quad (6)$$

The network’s inductance can be computed using the quality factor approach as:

$$Z_{in} = \frac{1}{jB + \frac{1}{(R_L + jX_L) + jX}} = R_s \quad (7)$$

$$Q = \frac{I_m(Z)}{R_e(Z)} = \frac{I_m\left(\frac{1}{jB + \frac{1}{(R_L + jX_L) + jX}}\right)}{R_e\left(\frac{1}{jB + \frac{1}{(R_L + jX_L) + jX}}\right)} \quad (8)$$

$$Q = B * R_s$$

From Equation (8), the susceptance  $B$  of the MN is given as:

$$B = \frac{1}{R_s} \left[ \sqrt{\frac{R_s}{R_{in}} - 1} \right], \text{ for } (B > 0, \text{ capacitance}) \quad (9)$$

The reactance value  $X$  can be computed using a parallel to series transformation by equating the equivalent imaginary component to zero as:

$$X = R_{in}Q - X_{in} = R_{in} \left[ \sqrt{\frac{R_s}{R_{in}} - 1} \right] - X_{in}, \text{ for } (X > 0, \text{ inductance}) \text{ and } (X < 0, \text{ capacitance}) \quad (10)$$

The results of the RF harvesters demonstrated with an MN outperform the results of the rectennas designed without one [201]. However, two elements' tuning is limited in the L-section MN design. This can be addressed by introducing a second L-section into the circuit. Hence, the MN of the circuits can be transformed into a  $\Pi$ -section, T-section, and  $\gamma$ -section. The authors in [201] exploit the performance of the RF harvester based on L-section and  $\Pi$ -section MN. The EH circuits developed with a  $\Pi$ -section MN outperform its L-section counterparts, which is attributed to the increase in degree-of-freedom and quality factor (QF) in the MN. This design operates at a frequency of 0.900 GHz. The authors in [202] further demonstrated better performance of the  $\Pi$ -section MN in the RFEH's design system. This design operates at a frequency of 2.450 GHz. The MN is realized using a cascaded  $\Pi$ -section to form a balanced BPF at the input of a bridge rectifier. Introducing the bridge rectifier degrades the performance of the overall circuit, which realizes 72.3% at a  $P_{in}$  of 18.5 dBm. Another MN technique based on the L-section and  $\Pi$ -section MN is reported by the authors in [203]. The RFEH circuit achieved a peak RF-to-DC PCE of 5% for a  $P_{in}$  of -30 dBm at 300-MHz. The authors in [204] used the concept of the L-section MN to realized an EH circuit at 24-MHz. A single band distributed L-section MN is reported by the authors in [205]. The RF harvester is matched to a six-stage Villard voltage multiplier at 0.900 GHz. The authors in [193] presented a rectenna that was implemented using a seven-stage voltage multiplier. A  $\Pi$ -MN is deployed to match the input impedance of the RF-rectifier at 0.900 GHz. A section of the  $\Pi$ -section MN using components, such as an amplifier and a diode, is modeled with the circuit's equivalent input impedance [206].

Similarly, a  $\Pi$ -section MN comprising L1, L2, and C1 matching elements is used to match the circuit's input impedance to a  $R_{av}$   $\Omega$  TL by dividing the reactance  $X_2$  of the inductor L2 into two parts,  $X_{2m}$  and  $X_{2n}$ , such that  $L2 = L_{2m} + L_{2n}$ , and  $X_2 = X_{2m} + X_{2n}$ . Thus, Section 1 ([206]) comprises a series inductor  $L_{2n}$  and a shunt capacitor C1 with a susceptance  $B_a$ , and Section 2 ([206]) consists of a shunt inductor L1 with a susceptance  $B_b$  and a series inductor  $L_{2m}$ . An arbitrary impedance  $R_v$  is introduced into the circuit to simplify the network.  $R_v$  is randomly selected to be less than the average received RF power  $R_{av}$  or circuit input impedance  $R_{in}$ .

Looking into Section 1 ([206]), the quality factor  $Q_a$  can be expressed as:

$$Q_a = \pm \left[ \frac{1}{R_v G_{in}} - 1 \right]^{\frac{1}{2}} \quad (11)$$

where  $G_{in} = R_{in}^{-1}$ .

The imaginary reactance of the source and the load are canceled and then compared with their respective real part to determine the MN parameters  $X_{2n}$  and  $B_a$  at a given  $f_o$  ( $\omega_o/2\pi$ ).

$$X_{2n} = R_v \left[ \frac{1}{R_v G_{in}} - 1 \right]^{\frac{1}{2}} \quad (12)$$

$$B_a = G_{in} \left[ \frac{1}{R_v G_{in}} - 1 \right]^{\frac{1}{2}} - B_{in} \tag{13}$$

$L_{2n}$  and  $C1$  are computed as:

$$L_{2n} = \frac{R_v}{\omega_o} \left[ \frac{R_{in}}{R_v} - 1 \right]^{\frac{1}{2}} \tag{14}$$

$$C1 = \frac{1}{\omega_o R_{in}} \left[ \frac{R_{in}}{R_v} - 1 \right]^{\frac{1}{2}} - C_{in} \tag{15}$$

where  $B_{in} = \omega_o C_{in}$  provides the input susceptance of the proposed circuit and  $\omega_o$  represents the angular operating frequency.

By looking into Section 2 ([206]) of the network, the quality factor  $Q_b$  is defined by:

$$Q_b = \pm \left[ \frac{R_{av}}{R_v} - 1 \right]^{\frac{1}{2}} \tag{16}$$

The elements  $B_b$  and  $X_{2m}$  of the network are obtained by:

$$B_b = \frac{1}{R_{av}} \left[ \frac{R_{av}}{R_v} - 1 \right]^{\frac{1}{2}} \tag{17}$$

$$X_{2m} = R_v \left[ \frac{R_{av}}{R_v} - 1 \right]^{\frac{1}{2}} - R_{in} \tag{18}$$

Thus,  $L1$ , and  $L_{2m}$  are given by:

$$L1 = \frac{R_{av}}{\omega_o} \left[ \frac{R_{av}}{R_v} - 1 \right]^{\frac{1}{2}} \tag{19}$$

$$L_{2m} = \frac{R_v}{\omega_o} \left[ \frac{R_{av}}{R_v} - 1 \right]^{\frac{1}{2}} - \frac{R_{in}}{\omega_o} \tag{20}$$

$L2$  is determined by combining Equations (14) and (20) as:

$$L2 = \frac{R_v}{\omega_o} \left[ \left( \frac{R_{av}}{R_v} - 1 \right)^{\frac{1}{2}} + \left( \frac{R_{in}}{R_v} - 1 \right)^{\frac{1}{2}} \right] - \frac{R_{in}}{\omega_o} \tag{21}$$

where the total  $Q$  is expressed as  $= Q_a + Q_b$ .

The authors in [110] demonstrated the use of a distributed L-section MN for harvesting RF signals at 2.450 GHz. Thus, this paper proposed the design of the distributed dual-band MN. An equivalent L-section MN coupled across an  $R_{av} \Omega$  TL comprising an L-shunt circuited stub (TL1) and an ITx (TL<sub>x</sub>) is modeled in this work [76]. Hence, the MN parameters TL1 and TL<sub>x</sub> will be explored in this section.

The TL<sub>x</sub> transformer's characteristic impedance ( $Z_x$ ) and the electrical length ( $\theta_x$ ) are initially computed. Hence, the TL<sub>x</sub> parameter steadily converts the imaginary part of the equivalent circuit input impedance  $Z_x$  from odd to symmetrical across the  $f_o$  while maintaining the real part nearly constant. The equivalent input impedances of the circuit  $Z_{in_e}$  are reported at  $R_{Le1} + jX_{Le1}$  and  $R_{Le2} + jX_{Le2}$  for the two operating frequencies,  $f_1$  and

$f_2$ , respectively. Thus, the electrical length and the characteristic impedance of  $TL_x$  are  $Z_{x1}$  and  $\theta_{x1}$  at  $f_1$ . From  $TL_x$ , the input impedance can be expressed as:

$$Z_{in\_e}(f_1) = Z_{x1} \left[ \frac{(R_{Le1} + jX_{Le1}) + jZ_{x1} \tan \theta_{x1}(f_1)}{Z_{x1} + j(R_{Le1} + jX_{Le1}) \tan \theta_{x1}(f_1)} \right] \tag{22}$$

$$Z_{in\_e}(f_2) = Z_{x1} \left[ \frac{(R_{Le2} + jX_{Le2}) + jZ_{x1} \tan \theta_{x1}(f_2)}{Z_{x1} + j(R_{Le2} + jX_{Le2}) \tan \theta_{x1}(f_2)} \right] \tag{23}$$

where  $\theta_{x1}(f_2)$  represents the electrical length at  $f_2$ . In addition,  $f_1$  and  $f_2$  are govern by a frequency ratio  $p$ , as  $p = f_2(f_1^{-1})$ , where  $f_2 > f_1$ . Hence,  $\theta_{x1}(f_1) = p^{-1}\theta_{x1}(f_2)$ .

Therefore, the equivalent input impedance of the circuit ( $Z_{in\_e}$ ) at  $f_1$  and  $f_2$ , is steadily converted into a complex conjugate by  $TL_x$ , as given by:

$$Z_{in\_e}|_{f_1} = [Z_{in\_e}|_{f_2}]^* \tag{24}$$

Thus,  $Z_{x1}$  and  $\theta_{x1}$  can be expressed as:

$$Z_{x1} = \left\{ (R_{Le1}R_{Le2} + X_{Le1}X_{Le2}) + \left[ \frac{X_{Le1} + X_{Le2}}{R_{Le2} - R_{Le1}} (R_{Le1}X_{Le2} - R_{Le2}X_{Le1}) \right] \right\}^{\frac{1}{2}} \tag{25}$$

$$\theta_{x1} = \frac{1}{1+p} \left[ \arctan \left\{ \frac{Z_{x1}(R_{Le1} - R_{Le2})}{(R_{Le1}X_{Le2} - X_{Le1}R_{Le2})} \right\} + q\pi \right], \tag{26}$$

for  $q = 0, 1, 3, \dots$

$q$  is selected to maintain the feasibility of the microstrip line in the design. Then, the values of  $Z_{x1}$  and  $\theta_{x1}$  are computed through Equations (25) and (26), at  $f_1$  and  $f_2$ , respectively. The input impedance of the proposed design can be determined through various circuit modeling techniques. Various circuit modeling techniques can be deployed to determine the input impedance of the design.

Secondly, the corresponding characteristic impedance  $Z_1$  and the electrical length  $\theta_1$  of TL1 are evaluated. TL1 cancels out the imaginary part of  $Y_{in\_e}$  while leaving the real part virtually constant where  $Y_{in\_e} = 1/Z_{in\_e}$ . Therefore, the equivalent electrical length and the characteristic impedance of TL1 are expressed by  $Z_1$  and  $\theta_1$  at  $f_1$  or  $\theta_2$  at  $f_1$ , respectively. The input admittance of the short-circuited L-shunt stub TL1 is denoted as  $Y_{in\_e1}(f_1) = 1/jZ_{x2}\tan\theta_{x2}(f_1)$ . The imaginary side of the circuit can be virtually minimized to zero by properly positioning the parameters of TL1. As stated earlier, the admittances at  $f_1$  and  $f_2$  are then conjugated through a transformer  $TL_x$ , which can be represented as  $G + jB$  and  $G - jB$ . To compensate for the imaginary part, the admittance of the short-circuited L-shunt stub TL1 is given as:

$$Y_{in\_e} = \begin{cases} \frac{1}{jZ_1 \tan \theta_1} = jB_1 & \text{at } f_1, \\ \frac{1}{jZ_1 \tan(p\theta_1)} = -jB_1 & \text{at } f_2. \end{cases} \tag{27}$$

From Equation (27),  $Z_1$  and  $\theta_1$  become:

$$Z_1 = [B_1 \tan(p\theta_1)]^{-1} \tag{28}$$

$$\theta_1 = \pi * [1 + p]^{-1} \tag{29}$$

Therefore, using Equations (28) and (29), the parameters of TL1 can be determined accordingly.

Table 3 summarizes some basic single-band and dual-band RFEH designs reported here in this work and their MN techniques.

**Table 3.** Comparison of some basic single-band and dual-band RFEH systems.

Ref. [...]	Electrical Size ( $\lambda_g$ ): Antenna/Rectifier (mm)	Frequency (GHz)	Peak PCE (%): $P_{in}$ (dBm)	Ambient Source	MN Technique	Substrate Antenna/RF-Rectifier	Diode
[50]	$2.76 \times 0.76/0.68 \times 0.8$	5.8	61 : 6	NA	Distributed open and short-circuited stubs	RO4003(3.55)	SMS-7630
[85]	NA/0.2 $\times$ 0.22	0.673	40 : -18.5	NA	Lumped L-Section	FR-4(NA)	HSMS-285B HSMS-285C
[90]	$0.52 \times 0.36/0.4 \times 0.3$	2.5/3.6	59, 41 : 2	NA	Distributed and multiple lumped L-sections	RO4003(3.38)	SMS-7630
[94]	$0.35 \times 0.35 \times 0.35$	0.915/2.45	37, 30 : -10	NA	Distributed stubs and lumped L-section and SSr	ARLON-25N(3.38)	SMS-7630
[110]	$0.52 \times 0.31/0.14 \times 0.24$	2.45	68 : 5	NA	Lumped L-section	FR-4(4.4)	HSMS-2850
[113]	$0.35 \times 0.21$	2.45	59 : 6	NA	Distributed and lumped L-section	FR-4 (4.4)	SMS-7630
[123]	$1.5 \times 1.72/0.9 \times 1.0$	2.45	75 : 20	NA	Lumped + Distributed multiple open stubs	FR-4(4.4)	HSMS-286B
[128]	$1.72 \times 1.21/0.82 \times 0.51$	2.43	13:10.4	NA	RCN with multiple lumped, and distributed open and short stubs	FR-4(4.4)/RO4350B(3.66)	HSMS-2860
[131]	$0.9 \times 0.63/0.75 \times 0.22$	0.9	60 : 0	NA	Distributed L-Section	FR-4(4.3)	HSMS-285C
[132]	$1.10 \times 0.62/4^* (0.43 \times 0.22)$	1.8	51 : -10	Yes	Single stub + Lumped SSr	RO4003(3.38)/RO5880(2.2)	HSMS-2850
[137]	$0.63 \times 0.75/NA$	0.9/1.8	63, 59 : 0	NA	Distributed and multiple lumped	DRA(10.2)/FR-4(4.3)	HSMS-285C
[142]	$1.6 \times 1.3$	2.45	50 : -17.2	NA	Internal MN elimination	RO6002(2.94)	HSMS-2852
[146]	$1.40 \times 1.4/0.60 \times 0.21$	2.45/5.0	15.5, 12.3 : 0	NA	Distributed stubs with IC	FR-4(4.4)	HSMS-286B
[182]	NA	0.9	5 : -25	Yes	Lumped L-section	NA	NA
[183]	$1.11 \times 1.11/4^* (0.34 \times 0.60)$	1.8	6.9 : -30	Yes	Lumped + Distributed L-section	RO4003(3.38)/RO5870(2.33)	SMS-7630
[184]	$1.51 \times 1.51/4^* (0.30 \times 0.12), 12^* (0.40 \times 0.20)$	0.9/1.8	57.5, 49.2 : -5, -10	Yes	Single stub + Lumped SSr	FR-4(4.4)/RO5880(2.2)	HSMS-2850
[186]	$3.45 \times 1.45/(0.88 \times 0.57)$	1.8/2.5	24 : -20	Yes	NA	FR-4(4.4)	HSMS-2850
[187]	$1.4 \times 0.51/NA$	2.45	NA	NA	Lumped L + Multiple distributed stubs	FR-4 (4.4)/RO4350(3.66)	SMS-202UP
[190]	NA	0.896	43 : -11	NA	Distributed stubs with CMOS	NA	NA
[196]	$0.62 \times 0.52/NA$	2.4	77.8 : 10	NA	Distributed II and L-section	RO5870(2.33)	HSMS-2820
[197]	$0.6 \times 0.5/NA$	0.8/0.9	30 : 0	NA	Multiple lumped L-section	FR-4 (4.7)	HSMS-2820 HSMS-2822
[202]	$2.9 \times 1.9$	2.45	72.3 : 19	NA	Distributed multi-stage stubs	ARLON-AD1000(2.35)	HSMS-2818
[203]	NA	0.435	30 : -10	NA	Lumped L and II-Section	NA	HSMS-285C
[207]	$0.53 \times 0.50/NA$	0.8/0.9	30 : 0	NA	Multiple lumped L-Section	FR-4(4.7)	HSMS-2820 HSMS-2822
[208]	$0.42 \times 0.42/NA$	5.5	74 : 40	NA	Distributed and lumped II-section	RO5880(2.2)/RO4003(3.38)	HSMS-2862
[209]	$1.6 \times 1.43$	2.45/5.8	84.4, 82.7 : 42, 38	NA	Distributed and multiple lumped band-pass	RO5870(2.33)	MA4E-1317
[210]	NA	5.8	60 : 12	NA	Multiple distributed open stubs	RO4003(3.38)	HSMS-2860
[211]	NA	5.8	74 : NA	NA	Multiple lumped band-pass	RO5880(2.2)	MA4E1317
[212]	NA/3.86 $\times$ 4.89	1.8/2.1	50 : NA	NA	RCN with distributed open and short-circuited stubs	ARLON-25N(3.38)	SMS-7630
[213]	$0.75 \times 0.60/0.80 \times 0.80$	2.4/5.8	63, 54.8 : 12.5	NA	Distributed open and short-circuited stubs	FR-4(4.4)	HSMS-2860
[214]	NA	0.914/2.4	43.1, 36.5 : 0	NA	RCN with distributed open stubs	FR-4(4.3)	NA
[215]	NA	0.9	70 : 5	Yes	L-Section + microstrip stubs	Taconic-TLX8(2.55)	HSMS-2852
[216]	NA	0.9/1.8	65.1, 55.2 : 0	NA	Distributed and multiple lumped	FR-4(4.3)	HSMS-2852
[217]	$0.9 \times 0.9/1.0 \times 0.62$	1.8	47 : 0	NA	Distributed open and shunt-circuited multiple stubs	RO3206(5.8)/RO3203(3.02)	SMS-7630
[218]	$1.03 \times 1.03/NA$	2.45	37.8 : -1.5	NA	NA	FR-4(4.4)	HSMS-286C
[219]	NA	0.915	25 : 1	NA	Lumped L-section	NA	HSMS-2862
[220]	$0.65 \times 0.71/0.76 \times 0.84$	2.45	8 : -15	NA	Distributed L-section	Paper(2.55)	HSMS-2850
[221]	NA	0.49/0.86	54.3 : -10	NA	Distributed, lumped resonator	FR-4(4.5)	NA

\*, Number of RF-rectifier or source antenna element in the rectenna system.

#### 4.2.2. Multi-Band and Wideband MN

This section highlights some of the important multi-band and wideband IMN approaches. The deployment of a multi-band RF harvester is described as a suitable approach toward having a durable RFEH system with a stable source of energy [222]. This is because of the RF signal tone contributed by each of the operating frequencies [222]. The authors in [221] reported the design of a dual-band RF-rectifier. The RF harvester is implemented using a cascaded segment of the L-section MN at 0.490 and 0.860 GHz. This design achieved a PCE of 54.3% for an  $P_{in}$  of -10 dBm. The authors in [136] developed a multi-band MN for an RFEH system. The multi-band characteristic is achieved by interconnecting several RF-rectifiers operating at a single band. A dual-band MN is demonstrated by the authors in [216] to harvest RF signals. The MN in the RF harvester is achieved with the help of a

fourth-order topology, which is configured as a series-parallel inductor capacitor circuit (LC). A T-section distributed MN is developed by the authors in [223]. A manually tuned MN is introduced in the design of an RF harvester by the authors in [2]. This RF harvester is realized by integrating the MN with trimmers to match the input impedance of the four-stage voltage multiplier. This work operates within the range of 0.700, 0.850, and 0.900 GHz spectra. A peak PCE of 41%, 40%, and 42% is observed across the three adjustable RF-rectifier operating frequencies for a  $P_{in}$  of 0 dBm, respectively. In the current trends that involve the management of a large volume of sensor networks and IoT devices, the design technique is impractical because of the maintenance expenses of manually matching the impedance of the source antenna with the RF-rectifier. A triple-band RF-rectifier is demonstrated by the authors in [224]. This design is realized by stacking open and short-circuited IMN stubs. This design matches the input impedance of the RF-rectifier using a cascaded ITx network at 0.850, 1.770, and 2.070 GHz. This work realized a peak PCE of 61.9%, 71.5%, and 60.5% for a  $P_{in}$  of 0 dBm, respectively. The authors in [144] reported the design of a differential RF harvester. The work operates at 2.000, 2.500, and 3.500 GHz. This work attained a maximum PCE of 53%, 31%, and 15.56% for a  $P_{in}$  of  $-7$  dBm, respectively. A triple-band RF harvester at 1.840, 2.140, and 2.450 GHz is introduced by the authors in [222]. A pair of the triple-band RF-rectifier is equally shared among the sixteen-port source antenna. A four-band RF-rectifier is presented by the authors in [225] operating at 0.890, 1.270, 2.020, and 2.380 GHz. The MN in this work is realized by adding a cross-shaped stub between a step-impedance TL. Then, two-radial stubs are integrated to establish the DC-pass filter network. Two diodes, HSMS-2850 D1 and HSMS-2860 D2, are assembled with a field effect transistor (FET) for DC conversion. The design reported a maximum PCE of 47.8%, 33.5%, 49.7%, and 36.2% for a  $P_{in}$  of  $-10$  dBm, respectively. Two separate RF-rectifiers were investigated by the authors in [226]. A quad-band RF-rectifier operating at 0.950, 1.830, 2.450, and 2.620 GHz is analyzed by the authors in [195]. This work deployed multiple combinations of TL and radial stubs to match the input impedance of the four-stage voltage multiplier. This design achieved a peak PCE of 44.8%, 27.5%, 28%, and 24.2% for a  $P_{in}$  of 10 dBm, respectively. Similarly, the cascaded MN reported by the authors in [195] for the multiple rectifying diodes significantly reduces the performance of the overall circuit. The RF-rectifiers are configured with common matching networks (CMN) and a two-branch MN (TBMN), each operating at 0.870 and 0.910 GHz, respectively. The CMN approach linked the MN with the source port and rectification section. The TBMN deployed the concept of a power divider at  $50 \Omega$  TL with an impedance of  $100 \Omega$  from each line. As a result, the two segments of the RF-rectifier are matched through a  $100 \Omega$  impedance. The designs achieved a PCE of 67.3% and 70.6% for a  $P_{in}$  of 16 mW, respectively. The authors in [227] presented a four-band RF harvester. Two separate RF harvesters were added using a DC-combining technique. The first segment of the design harvests frequency modulated (FM) signals at 98.00 MHz. The second segment of the design is achieved by designing a three-band RF-rectifier matched at 0.880, 1.700, and 2.370 GHz. The lower-FM RF harvester can only harvest RF signals in a direct line of sight (LOS), and the RF-rectifier is realized using a LC-section MN with a narrow BW of 10 MHz. This RF-rectifier attained a maximum PCE of 80% for a  $P_{in}$  of  $-6$  dBm. Conversely, the three-band RF-rectifier realized a maximum PCE of 77%, 74%, and 54% for a  $P_{in}$  of  $-6$  dBm, respectively. Hence, because of the RF-rectifier's limited BW, the design does not fully utilize a significant portion of the frequency BW in the spectrum. The large electrical length attributed to the overall circuit design and the introduction of a two-level DC-combiner further increased the TL losses. A six-order lumped element was configured into a three-segment to match the input impedance of the single-dual diode voltage multiplier by the authors in [228]. The design operates at 0.550, 0.750, 0.900, 1.850, 2.150, and 2.450 GHz. This work realized a maximum PCE of 67% for a  $P_{in}$  of  $-5$  dBm. Hence, the  $-10$  dB operational BW stated in the design is quite narrow over the target operating frequencies. The deployment of a single-dual-diode added parasitic capacitance to the overall circuit. Additionally, introducing a six-order filter in the MN across the three RF-rectifier segments decreases the

performance of the RF harvester. The authors in [229–232] used a similar design approach to design a multi-band MN. The work in [229] operates at 4.750, 5.420, 5.760, 6.400, 6.900, and 7.610 GHz, which are not suitable for the harvesting of RF signals in the ambient surrounding. Similarly, the work reported in [232] operates at 0.900, 1.800, 2.500, 3.500, 5.500, and 7.350 GHz, with an insignificant amount of RF signals for harvesting at 3.500, 5.500, and 7.350 GHz. In addition, the performance of these two RF harvesters is realized at high  $P_{in}$ . The designs reported by the authors in [195,223] are appropriate for a high-power RFEH system. Hence, the circuit's complexity contributed to the reduction in the overall circuit performance. The authors in [222,227] leverage the potential of a spatial domain through the concepts of either combining a multi-port or multiple antennas to enhance the RF-to-DC PCE of the RFEH system. The resulting rectifier output is merged using a DC-combining technique using a series of connecting terminals. As with the multiple antennae, the incoming RF signals are combined using a special RF-signal combiner. Then, the resulting signal is fed to the input terminal of the RF-rectifier through the MN. Hence, most of the MN designs that have been reported from the available literature for dual-band or multi-band operations are configured with a narrow operational BW that spans between 20 and 40 MHz [15,100,218,233,234].

Table 4 summarizes some basic multi-band RFEH designs reported here in this work and their MN techniques.

**Table 4.** Comparison of some basic multi-band RFEH systems.

Ref. [...]	Electrical Size ( $\lambda_g$ ): Antenna/Rectifier (mm)	Frequency (GHz)	Peak PCE (%): $P_{in}$ (dBm)	Ambient Source	MN Technique	Substrate Antenna/RF-Rectifier	Diode
[2]	NA/ 0.3 × 0.2	0.7/0.85/0.9	41,40,42 : 0	Yes	Lumped and distributed tunable	FR-4(4.6)	HSMS-285C
[136]	NA	0.9/1.8/2.1/2.45	15 : −20	Yes	Distributed and multiple lumped band-pass	RO4003(3.3)	MSS20-141
[139]	0.81 × 1.0/0.4 × 0.20	0.925/1.85/2.15	27,20,14 : −20	NA	Distributed open and short-circuited stubs + lumped SSr	RO3003(3.0)/RO5880(2.2)	SMS-7630
[144]	1.70 × 1.70/1.43 × 0.61	2/2.5/3.5	53,31,15.5 : 7	Yes	Pair of microstrip stubs	FR-4(4.4)	HSMS-285C
[195]	NA/1.23 × 0.51	0.9/1.8/2.1/2.45	45,27,28,24 : 10	NA	Pair of microstrip stubs	FR-4(4.1)	HSMS-2852
[222]	16 * (0.3 × 0.3)/0.4 × 0.8	1.84/2.14/2.45	25,3,27,9,19.3 : −20	Yes	Distributed open and short-circuited stubs	RO4003(3.38)/RO5880 (2.2)	HSMS-2850
[223]	NA/0.82 × 0.53	1.3/1.7/2.4/3.6	15 : −13	NA	Distributed, lumped resonator	FR-4(4.4)	SMS-7630
[224]	NA/0.30 × 0.11	0.85/1.77/2.07	61,9,71,5,60.5 : 0	NA	Open and short-circuited stubs	RO5880(2.2)	HSMS-2850
[225]	NA/ 0.64 × 0.44	0.89/1.27/2.02/2.38	47,8,33,5,49,7,36.2 : −10	NA	Cross-shape + stepped line impedance	F4B-2(2.65)	HSMS-2850 HSMS-2860
[227]	0.62 × 0.62/0.02 × 0.02/0.4 × 0.42	0.098/0.88/1.7/2.37	80,77,74,54 : −6	Yes	Lumped L-section, and distributed multi stub	FR-4(4.3)/RO4350B(3.48)	SMS-7630
[228]	0.3 × 0.3/ 0.1 × 0.12	0.55/0.75/0.9/1.85/2.15/2.45	67 : −5	Yes	Distributed and multiple lumped band-pass	FR-4(4.3)/RO5880(2.2)	SMS-7630
[229]	0.30 × 0.30/0.62 × 0.75	4.75/5.42/5.76/6.4/6.9/7.61	84 : 15	NA	Distributed and multiple lumped band-pass	FR-4(4.4)	HSMS-2820
[230]	NA/0.4 × 0.31	0.9/1.8/2.45	52, 50, 46.5 : 0	NA	Distributed stacked of open and short-circuited stubs	FR-4(4.4)	HSMS-2852
[232]	0.40 × 0.40/1.52 × 0.87	0.9/1.8/2.5/3.5	78 : 15	NA	Distributed and multiple lumped band-pass	FR-4(4.4)	HSMS-2820
[235]	0.50 × 0.3/0.11 × 0.14	0.94/1.95/2.44	80,46,42 : 10	NA	L-Section + inductor branch	RO4003(3.55)/FR-(4.4)	HSMS-285C
[236]	NA	0.5/0.9/1.8/2.1	40 : NA	Yes	Multiple lumped L-section	FR-4, PERSPEX	SMS-7630
[237]	0.260 × 0.25/0.11 × 0.14	2.45	NA	Yes	Distributed and a pair of lumped SSr	RO4003(3.38)/RO3206(6.6)	SMS-7630
[238]	0.7 × 0.7/NA	0.9/1.75/2.15/2.45	16 : −10	NA	Distributed open and short-circuited stubs	Taconic-TLP5(2.2)/TaconicRF60A(6.2)	SMS-7630
[239]	NA	0.6/2.4	55 : 3	NA	Distributed and a pair of lumped band-pass	ARLON-25N(3.7)	HSMX-282X
[240]	0.83 × 1.12/0.62 × 0.75	2.4/3.5/5.2	80 : 7	NA	Distributed open stubs	FR-4(4.4)	HSMS-282E

\*, Number of RF-rectifier or source antenna element in the rectenna system.

The authors in [241] used an octave-BW RF-rectifier design approach. The MN in this work is realized by interconnecting a non-uniform TL with an inductor in series. This design operates between 0.470 and 0.990 GHz. The design also attained an overall PCE of 5% for a  $P_{in}$  of −20 dBm. The authors in [242,243] transformed a wideband class-F1 power amplifier into a wideband RF-rectifier. This technique was achieved by incorporating feedback that generates a gate driving signal from the incoming RF-rectifier source terminal. This design produced a BW between 0.600 and 1.150 GHz with a maximum PCE of 60%. Despite

the performance improvement of this designed architecture across the target operating frequencies, the PCE is obtained at a high  $P_{in}$  of 40 dBm. The authors in [56] developed a broadband RF harvester to improve the overall circuit performance. With a maximum PCE of 55%, this device obtained a BW of 700 MHz between 1.800 and 2.500 GHz for a  $P_{in}$  of 10 dBm. Recently, a wideband CPW-based MN has been studied by the authors in [185]. This approach is achieved by adding a series of lumped elements to match an SSMx. This reported work operates between 1.000–1.850 GHz and 2.700–2.900 GHz with a peak efficiency of 45%. The drop in the overall PCE is associated with the high loss attributed to the CPW board. A broadband rectenna was reported by the authors in [244]. The two segments of the broadband MN are connected to the source terminal using a hybrid coupler. The RF harvester covers a frequency range of 1.500 to 2.600 GHz. This work was able to evaluate the rectenna performance across three operating frequencies comprising 1.810, 2.080, and 2.450 GHz.

Therefore, designing a single-band, dual-band, and multi-band or wideband RF-rectifier capable of operating over a wide range of frequency bands comprising GSM900/1800, UMTS/2100, LTE/2600, and ISM/Wi-Fi/2.4 is quite challenging due to the nonlinear characteristics of rectifying circuits controlled by: (I) Operating frequency(ies) ( $f_o$ ), (II) Input power ( $P_{in}$ ), (III) Diode nonlinear resistance ( $R_d$ ), and (IV) The terminal load ( $R_L$ ) [76,152,223,227]. Hence, broadband or wideband RF-rectifiers can be deployed to improve the  $P_{dc}$ . However, a tradeoff between PCE and electrical size or footprint must be taken into account [56,224,245–248].

Table 5 summarizes some basic wideband RFEH designs reported here in this work and their MN techniques.

**Table 5.** Comparison of some basic broadband/wideband RFEH systems.

Ref. [...]	Electrical Size ( $\lambda_g$ ): Antenna/Rectifier (mm)	Frequency (GHz)	Peak PCE (%): $P_{in}$ (dBm)	Ambient Source	MN Technique	Substrate Antenna/RF-Rectifier	Diode
[33]	NA/0.2 × 0.12	0.85–2.5	30 : 0	NA	Multiple lumped L-section	FR-4(4.4)	SMS-7630
[47]	0.6 × 0.25/0.5 × 0.2	0.9–3.0	73.3 : 3	NA	Distributed, lumped resonator	RO5880(2.2)	HSMS-2850
[56]	0.9 × 0.9/0.3 × 0.3	1.8–2.5	55 : –10	Yes	Distributed and multiple lumped band-pass	FR-4(4.4)/RO5880 (2.2)	SMS-7630
[84]	0.6 × 0.63/NA	1.975–4.744	22.7, 28.4 : 20	NA	NA	FR-4(4.4)	HSMS-270B
[148]	1.8 × 1.24/0.4 × 0.5	2.2–2.6	50 : 13	NA	Lumped and distributed stubs	F4B-2(2.65)	HSMS-2862
[150]	0.63 × 0.75/NA	0.9–5.5/0.9,1.8	60 : 0	NA	Lumped L-Section	FR-4(4.3)	HSMS-285C
[158]	1.72 × 1.72	5.3–6.1	73.4 : –6	NA	Lumped and distributed stubs	PTFE(2.1)	HSMS-2862
[159]	0.57 × 0.75/0.23 × 0.16	0.57–2.75	NA	Yes	Distributed stubs and multiple lumped	RO4003C(3.55)	NA(FET)
[160]	0.50 × 0.71/NA	2–3.1	70 : 5	NA	Distributed stubs + Lumped SSr	FR-4(4.4)	HSMS-2852
[164]	0.5 × 0.55/0.25 × 0.25	0.7–0.9	60 : 0	NA	Lumped and distributed stubs	Taconic-TLY5(2.2)	SMS-7630
[179]	NA/0.5 × 0.12	0.4–1.0	60 : 10	NA	Non-uniform TL + lumped	ARLON-A25N(3.38)	SMS-7630
[185]	NA/0.23 × 0.27	1.0–1.85, 2.7–2.9	74 : 10	NA	Lumped and distributed stubs	FR-4(4.4)	SMS-7630
[241]	NA/0.65 × 0.22	0.47–0.86	60 : 10	NA	Non-uniform TL + lumped	ARLON-A25N(3.38)	SMS-7630
[242]	NA	0.6–1.15	79 : 20	NA	Distributed and lumped class F-1 PA	NA/RO4350	NA
[244]	1.0 × 1.92/1.26 × 0.72	1.55–2.60	50 : –5	NA	Pair of microstrip multiple stubs	FR-4(4.4)/Taconic-TLY5A(2.17)	SMS-7630
[249]	NA	2.00–18.00	20 : –7	NA	Hybrid multi-stage	NA	SMS-7630
[250]	NA	0.9–1.1, 1.8–2.5	75 : 20	NA	Lumped and distributed tunable	RO6002(2.94)	SMS-7630 HSMS-2860
[251]	0.42 × 0.4/0.5 × 0.2	1–5	61 : 9	NA	BALUN + Distributed differential TL stubs	FR-4(4.4)	SMS-7630
[252]	1.8 × 1.8	1.8–2.6	50 : 5	NA	Non-uniform meandered TL	FR-4(4.3)	SMS-7630
[253]	0.54 × 0.54/0.54 × 1.7	29–46	80 : 2	NA	Distributed stubs	RO5880(2.2)	NA(GFET)
[254]	0.54 × 0.54	1.1–2.7	80, 75, 70 : 12	NA	Lumped and distributed tunable	RO5880(2.2)	HSMS-2852

#### 4.3. RF-Rectifier Circuit

After the transformation of the incoming RF signals through the IMN, an RF-rectifier (rectifier/multiplier) is deployed to convert the input signal to a DC source. In addition, it also enhances the voltage from the receiving antenna to a usable level through a proper rectenna management operation [180]. The primary objective for the low-power RF-rectifier

and sensing unit is to retrieve the highest number of the available RF signals and limit the loss of power generated through the components following the rectification process.

Rectifiers are divided into half-wave and full-wave rectifiers depending on their design architecture, which can be further classified according to their applications and purpose. As a result, it is important to enhance the RF-rectifier performance in order to realize the conversion of the low RF ambient signals at high efficiency. Various studies have demonstrated that when the intercepted RF power is low, so is the rectifier's overall PCE [251]. Hence, analysis of various rectifier design techniques is going to be discussed in this section for a better understanding of efficient RF-rectifiers design.

#### 4.3.1. Half-Wave Rectifiers

Half-wave rectifiers are also called half-wave rectifier circuits (HW-R). During the conduction process, only a half-wave of the incoming AC signal is taken into consideration for the DC signal conversion. HW-R can be further categorized into a shunt-HW-R and series-HW-R under the load and rectifying diode configuration. An RF harvester design based on HW-R configuration uses a lower amount of  $P_{in}$ . This is because of the single diode with reduced parasitic junction capacitance, making it appropriate for low-power RFEH applications. The authors in [224] have successfully demonstrated the use of HW-R for improved RF-to-DC PCE. To improve rectifier performance, a Wilkinson power divider using a pair of HW-R circuits is employed by the authors in [255,256]. The RF signal angle of incidence does not affect this designed technique. The authors in [217] investigate the same technique for power splitting and power combining. This approach claims to have improved the rectifier's performance by minimizing power management issues with improved sensitivity. The authors in [224,257,258] demonstrated that the SSr-diode configuration has shown an improved performance for low RF power operation less than 0 dBm. Generally, as the  $f_o$  of the rectifier increases, the PCE of the RF-rectifier decreases and vice versa [15,219,220]. The operation of the HW-R in the RF-rectifier circuit is described from the point of signal interception by the receiving antenna. This signal is transmitted and transformed into DC by the rectification section. During the positive half-cycle, the series-HW-R conducts and allows the flow of signal to the  $R_L$  through the DC-pass capacitor filter. The signal gets blocked by the SSr configuration in the negative half-cycle. Hence, the shunt-HW-R undergoes the same operation procedure in reverse order. Therefore, the deployment of the HW-R topology draws less power during the conversion process because of the single diode operations with less junction capacitance and forward bias voltage. This makes the configuration suitable for low-power applications. Hence, the issues of the low output power can be addressed through the concept of full-wave rectifiers at the cost of the reduced circuit's PCE.

#### 4.3.2. Full-Wave Rectifiers

Full-wave rectifiers are also called full-wave rectifier circuits (FW-R). This technique simultaneously considers the positive half-cycle and the negative half-cycle during the DC conversion process. This configuration approach is classified into full-wave bridge rectifiers and voltage multipliers. The voltage multipliers are further configured according to the cascade levels and the arrangement of the capacitors at the common ground level. The authors in [180] presented various cascade topologies of the FW-R according to the Dickson or Greinacher and Villard or Cockroft–Walton cascaded configurations. The authors in [221] developed a dual-band RF-rectifier at 0.490 and 0.860 GHz. The RF harvester is realized using a voltage multiplier. The authors in [259] investigate the development of an RF-rectifier using a SSMx. The RF-rectifier operates at 0.980 and 1.800 GHz and achieved a maximum PCE of 60% and 17%, respectively.

A CPW-based RF-rectifier is presented by the authors in [185]. The design is implemented using an SSMx. The authors in [260] illustrate the concept of voltage multiplication using a cascaded topology at 0.953 GHz. This RF harvester shows an improvement in the overall output voltage at the cost of low PCE. The authors in [41] show a similar kind of

outcome. The authors in [252] described the design of an RF harvester circuit that can work across a wide frequency range using a voltage multiplier topology. The SSMx is matched through a non-uniform TL connection to achieve the wideband operation. The authors in [251] deployed the concept of SSMx based on a differential circuit model to enhance the PCE of the RF harvester while maintaining a steady balance of the  $V_{dc}$  supply. The authors in [56,229,240,261–264] further explore the concept of RF-rectifier design based on Greinacher architecture. The rectifier implemented by the authors in [56] operates between 1.800 and 2.500 GHz. In addition, the authors in [263] employ a hybrid rat race coupler for harvesting energy. The design was able to provide a  $180^\circ$  phase difference to match the input impedance of the Greinacher rectifying section. The authors in [265] developed an RFEH circuit architecture based on a rectifier regulator-booster (RBR). A Greinacher and a Cockcroft–Walton charge-pump rectifier topology were used to achieve the desired RBR architecture at 2.450 GHz. The RF-rectifier achieves a maximum PCE of 85% for a  $P_{in}$  of 20 dBm, making it suitable for high-power applications. A FW-R-bridged architecture is an appropriate circuit configuration for high RF power operations above 15 dBm. The shunt-diode architecture, on the other hand, is appropriate for deployment in the medium RF power levels between 0 and 15 dBm.

#### 4.3.3. Other Topologies for Rectifiers and Overview

The PCE of the RF-rectifier is a generic representation of the RFEH circuit's performance in any form of topology. To minimize the circuit sensitivity with respect to the  $R_L$  and mitigate the effects of impedance mismatch, several methods, such as the resistance compression network (RCN) and adaptive RF-rectifier circuits, are implemented. The authors in [266] demonstrated the concept of the RCN. The compression network makes the RF-rectifier circuit look like a constant resistance load, regardless of  $P_{in}$  or  $V_{dc}$ . RCN makes the  $R_L$  impedance of the RFEH circuit behave closely to that of the fixed terminal load, regardless of the incoming RF signals or the conditions of the  $V_{dc}$ . The authors in [212] reported an RF harvester using a RCN design approach at two operating frequencies. The RCN is realized at 0.915 and 2.450 GHz with limited sensitivity. However, it is more sensitive to impedance variations at the input of the rectification unit than at the RF source. The RCN-based RF-rectifiers reported by the authors in [212,266] are achieved using lumped elements. Hence, a distributed TL-based RCN can be deployed to overcome the overall circuit performance of the conventional RCN, because the TL-based RCN distributes the incoming RF signals evenly across the design's multiple components. This is useful when managing an RF-rectifier with a low power capability, as reported by the authors in [267].

The authors in [268] reported an RF harvester configured by integrating a diode with a metal oxide semiconductor field effect transistor (MOSFET). It is discovered that the designed approach reduces the RF-rectifier's turn-on voltage at 2.450 GHz. During the design process, a FW-R configuration with five stages is introduced into the network to enhance the overall circuit performance. The operation of the adaptive MOSFET RF-rectifier is investigated by the authors in [269] over a wide range of the incoming RF signal levels. The adaptive RF-rectifier shows an improvement in the overall PCE across the wide range of the  $P_{in}$ . The design realized a peak PCE of 75% for a  $P_{in}$  of 15 dBm at 100.00 MHz. The authors in [270] presented a 2.450 GHz adaptive RF-rectifier with a wider range of  $P_{in}$ . The broadband MN is achieved by deploying an additional circuit control unit. This device is constructed based on the complementary metal oxide semiconductor (CMOS) technology and has attained a maximum PCE of 47%. The authors in [253] examined an RF harvester using a graphene-based field effect transistor (GFET) architecture. The design is realized for millimeter-wave (mm-wave) applications between 29.00 and 46.00 GHz. The design shows an overall PCE improvement of 80.32% for a  $P_{in}$  of 1.6 mW. To obtain a lower threshold voltage ( $V_{TH}$ ) and a large  $V_{br}$ , the authors in [271] use another approach to design an RF-rectifier architecture. The design achieved a dual-band  $f_o$  at 0.915 and 1.800 GHz with a

peak PCE of 60% for a  $P_{in}$  of 15 dBm. This method claims to have minimized the chances of a rapid  $V_{br}$ .

One of the Schottky diode's constraints is the switching speed, which can be addressed by the MOSFET's technology. However, the MOSFET devices require a higher turn-on voltage than their Schottky diode counterparts, and the MOSFET chips are susceptible to thermal overheating. Hence, a tradeoff made between the two components considers the deployment of the Schottky diode for a low-power RFEH system [2,13,15,30,36,100,148,186,223,228,272–276].

The RF  $P_{in}$  has a significant impact on the rectenna RF-to-DC PCE. This effect is observed to decrease the rectenna PCE drastically when the incoming voltage remains lower than the diode threshold ( $V_{th}$ ) or turn-on voltage over time. This is associated with the diode's IV-curve exponential characteristics. Thus, a rectifying diode with a high  $V_{br}$  and a minimum  $V_{th}$  is a suitable component for an efficient RF-rectifier design. This facilitates fast switching operation at the diode junction. A diode with a higher saturation current ( $I_s$ ) also enhances the forward bias current ( $I_f$ ), which is convenient for driving the terminal load. The diode's  $I_s$  influences the parallel resistance of the RFEH diode. The diode's parallel resistance decreases as  $I_s$  increases, making it suitable for applications with low operating frequencies [277]. Additionally, the diode resistance ( $R_d$ ) decreases, allowing the rectifying diode to conduct at low RF power levels. However, the  $I_s$  depends on the barrier width of the RFEH diode. However, a higher  $I_s$  is often seen in diodes with large dimensions, which increase the junction and substrate capacitance [36,84]. A diode with a low barrier height produces a low voltage drop, and a significant amount of reverse leakage current ( $I_{rv}$ ) flows through the junction of the barrier diode, which lowers the diode's  $V_{th}$  voltage. These two variables can lead to additional power loss, which negates the advantage of higher  $I_s$  [96,260]. Hence, low power level transmission involves the use of a rectifying diode with a high  $I_s$  for easy RF harvester operation. It is also critical to extract the values of  $R_L$  of a given RFEH complex circuit, as this has a significant influence on the overall circuit's performance. However, realizing these properties in the same rectifying diode model is challenging. Relatively, the rectifying diode with increased  $I_s$  exhibits improved PCE [92,218,278]. As traditional diodes are incompatible with radio frequencies, diode families, such as Schottky diodes, are deployed to address the design of RF-rectifiers. Different classes of Schottky diodes for RFEH applications were investigated in this work. The MA-4E1317, SMS-7630, and HSMS-28xx are the most commonly used diodes for RFEH applications. The authors in [110] described the deployment of an SSMx for low RF power operation. The RF harvester is configured using an HSMS-2850 diode. The circuit realizes a peak PCE of 68% for a  $P_{in}$  of 5 dBm at 2.450 GHz. The authors in [279–281] investigate the performance of the SMS-7630 and HSMS-2860 diodes for an efficient RFEH system. The two diodes are analyzed within the power range of  $-40$  to 5 dBm. The RF harvester design using the SMS-7630 diode by the authors in [279] demonstrates a better efficiency compared to that of the HSMS-2860 counterpart. The design realizes a peak PCE of 42.10% and 42.50% for a  $P_{in}$  of  $-10$  dBm at 2.400 and 3.500 GHz, respectively. However, the performance of the SMS-7630 diode is significantly reduced when exploited over high operating frequencies [2,15,94,141,228]. The authors in [254] described that the configuration setup of the SSMx RF harvester using an HSMS-2850 diode needs lower RF input signals to operate than that of the SMS-7630. The  $V_{br}$  of the HSMS-28xx diode series varies from 3.80 to 15.00 V [84,180,282–285]. With a minimum RF power level greater than  $-40$  dBm, these diode series can handle both high and low RF power levels. Similarly, the  $V_{br}$  of the MA-4E1317 rectifying diode is 7.00 V, making it ideal for applications where the RF power level exceeds 0 dBm [209,211,230,264,286,287]. Some of the commonly used electrical specifications of the Schottky RF diode models for enhanced PCE in RFEH applications are summarized in Table 6.

**Table 6.** Electrical specifications of some basic Schottky RF diode models deployed in the RFEH system.

Ref. [...]	Vendor	Model	$R_s$ ( $\Omega$ )	$I_s$ ( $\mu\text{A}$ )	$C_{j0}$ (pF)	$V_{th}$ (V)	$V_{br}$ (V)
[84]	Avago/BROADCOM	HSMS-2700	0.650	0.14	6.700	0.600	15.00
[207,229]	Avago/BROADCOM	HSMS-2820	6.00	0.022	0.700	0.150	15.00
[47,110,186,225],	Avago/BROADCOM	HSMS-2850	25.00	3.00	0.180	0.150	3.800
[195,215,216,254]	Avago/BROADCOM	HSMS-2852	25.00	3.00	–	0.150	3.800
[128,210,213,250]	Avago/BROADCOM	HSMS-2860	6.00	0.050	–	0.250	7.00
[123,146]	Avago/BROADCOM	HSMS-286B	6.00	0.050	0.180	0.690	7.00
[50,56,183,238]	Skyworks Solutions	SMS-7630	20.00	5.00	0.140	0.090	2.00
[209,211]	MACOM Partners	MA-4E1317	4.00	0.100	0.020	0.700	7.00
[136]	MACOM Partners	MSS20-141	–	–	0.080	0.500	0.800

The authors in [288] have studied a hybrid power harvesting technique to improve the PCE of the RFEH system. Here, mechanical vibration and EM wave radiation are exploited as potential candidates for EH systems. Conversely, an integrated EH approach studied by the authors in [289] is used to increase the PCE of the RF-rectifier at low  $P_{in}$  levels by combining two uncorrelated sources of energy. However, combining the uncorrelated energy sources adds to the overall circuit complexity. The authors in [290] demonstrated the performance evaluation of the multi-stage RF harvester implemented using HSMS-2822 and HSMS-2552 Schottky diodes. The configuration of the SSMx shows a better PCE for a  $P_{in}$  of  $-20$  dBm. It was reported by the authors in [290] that the increment in the number of the RF-rectifier stages improves the overall performance of the circuit at the cost of high  $P_{in}$ . The design attained a peak PCE and output  $V_{dc}$  through the nine-stage FW-R for a  $P_{in}$  of 10 dBm. However, the operation of the RF harvester at low RF  $P_{in}$  levels is zero, as the elements of the circuit drain the received incident power. As a result, when the number of RF-rectifier stages increases, the performance of the overall circuit is significantly degraded at low  $P_{in}$  levels because of the component losses [290]. Furthermore, a significant decrease in the RF-rectifier PCE is observed when the  $R_L$  is too high or small. It has also been discovered that an RF harvester configured for low-power applications works effectively with the fewest possible number of the source antenna elements. High-power design performance, on the other hand, is desirable with an increase in the number of antenna elements. Rectifying diode(s) deployed for RFEH applications should be considered properly for efficient EH, because certain diodes consume or drain a lot of energy and can affect the performance of low-power devices in the future.

#### 4.4. DC-Pass Filter

A DC-pass filter, also referred to as a pre-rectifier, is deployed to reduce the higher-order harmonics and smooth the peaks generated by the nonlinear portion of the rectifying diode(s) [56,213,215,291,292]. The transmission RF signals need simple circuitry for converting and storing the available ambient energy [293]. This can be accomplished through the optimization interface between the rectifying diode and the  $R_L$ . This introduction of a DC-pass filter between the two segments based on either distributed elements [41,226] or conventional storage units, such as capacitors [185,252,294–296], is the most commonly used approach for the RFEH circuit. The primary target is to maximize the overall PCE by reducing distortions and signal reflections [297]. For this reason, a reactive MN couples the antenna source with the RF-rectifier for optimal transfer of the received energy into the system [298]. The role of the DC-pass filter is to prevent the higher-order harmonics generated by the rectifying diode(s) and also contribute to the matching between the antenna source and the RF-rectifier. The DC-pass filter is deployed into the design of a multi-band or wideband RF harvester to facilitate the realization of the multiple signal tones by stacking two or more sub-rectifiers. The authors in [209] added an LPF and a pair of BSFs to reject the higher-order harmonics from a dual-frequency EH circuit. The authors in [202] use a bandpass filter (BPF) to block the higher-order harmonics of the differential

RF-rectifier because this signal is sometimes re-radiated back to the source, which affects the performance of the overall circuit. Various DC-pass filter design techniques have been covered in the available literature of this work to improve the overall performance of the RFEH system.

## 5. Emerging RFEH Studies

Based on the findings and the proposed design challenges, future studies can further investigate and improve on the following aspects:

Biomedical implants:

- The employment of flexible substrates, such as paper, polyethylene terephthalate (PET), and textile, can be one of the potential research areas for prospective RFEH harvesters in biomedical implantable devices for BAN applications. The attributes of the material pave the way for the design of a low-profile and conformal rectifier. The level of the DC power realized by a single band or multi-band rectenna can be addressed by cascading multiple RF-rectifier elements through the concept of DC combining;

5G technology:

- As 5G and 6G communications evolve, a significant part of potential research in wireless communication systems will either operate or harmonize the spectrum of the mm-wave and sub-millimeter waves. Hence, it is equally important to extend the scope of this research study to accommodate higher frequency bands such as 28, 38, and 60 GHz. Therefore, the proposed RF harvesters demonstrated in this work can be further investigated to address the effects of component loss at the extremely high operating frequency(ies).

Diode Model:

- The advancement of a low-power rectifying diode is a potential key study area in promoting RFEH technology. Fewer losses, low series resistance ( $R_s$ ), enhanced  $I_s$ , high forward bias voltage ( $V_f$ ), and a junction impedance or capacitance are some characteristics that need to be further explored;

Rectenna reconfigurability:

- To improve the level of the ambient RF signals, the concept of dynamic and reconfigurable rectenna arrays can be investigated. An RF and DC combining technique can be deployed, and the array pattern and beam orientation can be modeled as a self-reconfigurable and adaptable module to manage the real-time conditions of the RF signals;

Miniaturized Optical Rectenna:

- EH from infrared and other forms of visible lights can be investigated in the future using miniaturized optical rectenna. However, the technique suffers from poor PCE due to simple design requirement at optical  $f_o$  without provision for MN. The use of a high-impedance reconfigurable antenna is one of the proposed approaches to address this challenge;

Hybridization:

- The present rectenna module results in a  $V_{dc}$  level that makes it difficult for Big Tech companies to commercialize RFEH technology. Hence, the use of hybrid renewable energy harvesting (HREH) technology might revolutionize the process. HREH can be accomplished from diverse renewable energy sources that work in tandem. Therefore, automobiles, military and security surveillance, WSN, biomedical implantable devices, aircraft, wearable devices, and a variety of other platforms can all benefit from HREH technology.

## 6. Conclusions

The technique of the RFEH system has received a lot of interest from multiple scholars. The RF harvester is realized based on some primary design phases. First, the level of ambient power with the respective operating frequencies needs to be specified through the employment of the RF-spectral site survey. To develop an efficient low-power rectenna system, it is important to study, examine, and carefully specify all the relevant elements of the system according to the design specifications. This paper discussed the fundamental building blocks of the RFEH system for the evolving technology. Detailed research findings on the rectennas for low-power RFEH applications have been outlined and analyzed. Then, this is followed by the design and development of a suitable rectenna for RF-to-DC energy transformation. Furthermore, this study shows that Schottky diodes are among the suitable candidates for harvesting low-power RF signals, besides the deployment of self-biasing MOSFETs. The findings exploited in this work will help to establish a good understanding of the state-of-the-art rectenna designs. This work also helps identify some challenges that can be addressed in various studies. Most of the current trends in low-power RF harvesters reported in the available literature were found not to concentrate on a multi-band or broadband and 5G mm-wave rectenna system. Hence, this research has emphasized the significance of developing an RFEH component with a wide range of operating frequencies and varying  $P_{in}$  levels. Thus, a systematic design approach of an mm-wave RFEH module incorporating the co-design components of the rectenna on state-of-the-art PCB packaging technology and affordable semiconductors is desirable. Additionally, unique antenna design technologies, such as antenna-in-package, paired with integrated CMOS level design, are critical to enabling widespread mm-wave RF power systems.

**Author Contributions:** S.M., Design technique; S.M., A.S., M.I.W., implementation on software's; S.M., evaluation and validation; S.M., A.H.R., I.A., M.N.M.Y., A.S., M.I.W., A.S.A., formal examination; S.M., investigation; S.M., J.J.T., A.I., S.K.W., A.S., A.S.A., A.H.R., supplies and resources; J.J.T., S.K.W., I.A., M.N.M.Y., A.S., M.I.W., A.H.R., collections of data; S.M., composing—first and preparations of draft; S.M., I.A., M.N.M.Y., A.S., M.I.W., A.S.A., composing, reviewing, and editing; S.M., J.J.T., S.K.W., A.I., visibility; S.M., J.J.T., S.K.W., I.A., M.N.M.Y., A.H.R., A.S., M.I.W., supervisory; J.J.T., S.K.W., A.H.R., I.A., M.N.M.Y., A.S., M.I.W., A.S.A., management of a project. All authors have read and agreed to the published version of the manuscript.

**Funding:** TM R&D Malaysia funded this research with the MMUE/190001 grant code.

**Acknowledgments:** The authors acknowledge the financial support provided by Ministry of Higher Education through the Fundamental Research Grant Scheme (FRGS) under a grant number of FRGS/1/2020/TK0/UNIMAP/02/70.

**Conflicts of Interest:** The authors declared no conflict of interest regarding the originality of the proposed design.

## References

1. Caselli, M.; Tonelli, M.; Boni, A. Analysis and design of an integrated RF energy harvester for ultra low-power environments. *Int. J. Circuit Theory Appl.* **2019**, *47*, 1086–1104. [[CrossRef](#)]
2. Muncuk, U.; Alemdar, K.; Sarode, J.D.; Chowdhury, K.R. Multiband ambient RF energy harvesting circuit design for enabling batteryless sensors and IoT. *IEEE Internet Things J.* **2018**, *5*, 2700–2714. [[CrossRef](#)]
3. Niotaki, K.; Collado, A.; Georgiadis, A.; Kim, S.; Tentzeris, M.M. Solar/electromagnetic energy harvesting and wireless power transmission. *Proc. IEEE* **2014**, *102*, 1712–1722. [[CrossRef](#)]
4. Assimonis, S.D.; Daskalakis, S.N.; Bletsas, A. Sensitive and efficient RF harvesting supply for batteryless backscatter sensor networks. *IEEE Trans. Microw. Theory Tech.* **2016**, *64*, 1327–1338. [[CrossRef](#)]
5. Kim, S.; Vyas, R.; Bito, J.; Niotaki, K.; Collado, A.; Georgiadis, A.; Tentzeris, M.M. Ambient RF energy-harvesting technologies for self-sustainable standalone wireless sensor platforms. *Proc. IEEE* **2014**, *102*, 1649–1666. [[CrossRef](#)]
6. Basir, A.; Yoo, H. Efficient wireless power transfer system with a miniaturized quad-band implantable antenna for deep-body multitasking implants. *IEEE Trans. Microw. Theory Tech.* **2020**, *68*, 1943–1953. [[CrossRef](#)]
7. Shafique, K.; Khawaja, B.A.; Khurram, M.D.; Sibtain, S.M.; Siddiqui, Y.; Mustaqim, M.; Chattha, H.T.; Yang, X. Energy harvesting using a low-cost rectenna for Internet of Things (IoT) applications. *IEEE Access* **2018**, *6*, 30932–30941. [[CrossRef](#)]

8. La Rosa, R.; Livreri, P.; Trigona, C.; Di Donato, L.; Sorbello, G. Strategies and techniques for powering wireless sensor nodes through energy harvesting and wireless power transfer. *Sensors* **2019**, *19*, 2660. [[CrossRef](#)] [[PubMed](#)]
9. Nikandish, G.; Staszewski, R.B.; Zhu, A. Breaking the bandwidth limit: A review of broadband Doherty power amplifier design for 5G. *IEEE Microw. Mag.* **2020**, *21*, 57–75. [[CrossRef](#)]
10. Wagih, M.; Weddell, A.S.; Beeby, S. Millimeter-wave power harvesting: A review. *IEEE Open J. Antennas Propag.* **2020**, *1*, 56–578. [[CrossRef](#)]
11. Riaz, A.; Awais, M.; Farooq, M.M.; Khan, W.T. A single cell dual band rectifier at millimeter-wave frequencies for future 5G communications. In Proceedings of the 2019 49th European Microwave Conference (EuMC), Paris, France, 1–3 October 2019; pp. 41–44.
12. Jilani, S.F.; Munoz, M.O.; Abbasi, Q.H.; Alomainy, A. Millimeter-wave liquid crystal polymer based conformal antenna array for 5G applications. *IEEE Antennas Wirel. Propag. Lett.* **2018**, *18*, 84–88. [[CrossRef](#)]
13. Vuong, T.P.; Bui, D.H.N.; Verdier, J.; Allard, B.; Benech, P.; Design and measurement of 3D flexible antenna diversity for ambient RF energy scavenging in indoor scenarios. *IEEE Access* **2019**, *7*, 17033–17044.
14. Andrae, A.S.; Edler, T. On global electricity usage of communication technology: Trends to 2030. *Challenges* **2015**, *6*, 117–157. [[CrossRef](#)]
15. Divakaran, S.K.; Krishna, D.D. RF energy harvesting systems: An overview and design issues. *Int. J. RF Microw. Comput.-Aided Eng.* **2019**, *29*, e21633. [[CrossRef](#)]
16. Xu, J.; Ricketts, D.S. An efficient, watt-level microwave rectifier using an impedance compression network (ICN) with applications in outphasing energy recovery systems. *IEEE Microw. Wirel. Components Lett.* **2013**, *23*, 542–544. [[CrossRef](#)]
17. Leonov, V. Thermoelectric energy harvesting of human body heat for wearable sensors. *IEEE Sens. J.* **2013**, *13*, 2284–2291. [[CrossRef](#)]
18. Liu, X.; Ansari, N. Toward green IoT: Energy solutions and key challenges. *IEEE Commun. Mag.* **2019**, *57*, 104–110. [[CrossRef](#)]
19. Nguyen, C.V.; Nguyen, M.T.; Quyen, T.V.; Le, A.M.; Masaracchia, A.; Nguyen, H.T.; Nguyen, H.P.; Nguyen, L.D.; Nguyen, H.T.; Nguyen, V.Q. Hybrid solar-RF energy harvesting systems for electric operated wheelchairs. *Electronics* **2020**, *9*, 752. [[CrossRef](#)]
20. Roundy, S.; Wright, P.K.; Rabaey, J. A study of low level vibrations as a power source for wireless sensor nodes. *Comput. Commun.* **2003**, *26*, 1131–1144. [[CrossRef](#)]
21. Chin, C.H.; Xue, Q.; Chan, C.H. Design of a 5.8-GHz rectenna incorporating a new patch antenna. *IEEE Antennas Wirel. Propag. Lett.* **2005**, *4*, 175–178. [[CrossRef](#)]
22. Khan, D.; Oh, S.J.; Yeo, S.; Ryu, Y.; In, S.; Rad, R.E.; Ali, I.; Pu, Y.G.; Yoo, S.S.; Lee, M.; et al. A Solar/Triboelectric/RF Hybrid Energy Harvesting based High Efficiency Wireless Power Receiver. *IEEE Trans. Power Electron.* **2021**, *36*, 11148–11162. [[CrossRef](#)]
23. Tesla, N. Experiments with alternate currents of very high frequency and their application to methods of artificial illumination. *Trans. Am. Inst. Electr. Eng.* **1891**, *8*, 266–319. [[CrossRef](#)]
24. Khan, D.; Oh, S.J.; Shehzad, K.; Basim, M.; Verma, D.; Pu, Y.G.; Lee, M.; Hwang, K.C.; Yang, Y.; Lee, K.Y. An efficient reconfigurable RF-DC converter with wide input power range for RF energy harvesting. *IEEE Access* **2020**, *8*, 79310–79318. [[CrossRef](#)]
25. Yildiz, F. Potential Ambient Energy-Harvesting Sources and Techniques. *J. Technol. Stud.* **2009**, *35*, 40–48. [[CrossRef](#)]
26. Bashir, S.; Batool, S.; Imran, M.; Ahmad, M.I.; Malik, F.M.; Ali, U. Development of Frequency Weighted Model Reduction Algorithm with Error Bound: Application to Doubly Fed Induction Generator Based Wind Turbines for Power System. *Electronics* **2021**, *10*, 44. [[CrossRef](#)]
27. Parivar, H.; Shivaie, M.; Darahi, A.; Ansari, M. An Efficient Direct Torque Control Strategy for a Doubly Fed Induction Generator (DFIG) in Wind Energy Conversion Systems. In Proceedings of the 2021 IEEE Texas Power and Energy Conference (TPEC), College Station, TX, USA, 2–5 February 2021; pp. 1–5.
28. Visser, H.J.; Vullers, R.J. RF energy harvesting and transport for wireless sensor network applications: Principles and requirements. *Proc. IEEE* **2013**, *101*, 1410–1423. [[CrossRef](#)]
29. Lin, Y.L.; Zhang, X.Y.; Du, Z.X.; Lin, Q.W. High-efficiency microwave rectifier with extended operating bandwidth. *IEEE Trans. Circuits Syst. II Express Briefs* **2017**, *65*, 819–823. [[CrossRef](#)]
30. Singh, J.; Kaur, R.; Singh, D. Energy harvesting in wireless sensor networks: A taxonomic survey. *Int. J. Energy Res.* **2021**, *45*, 118–140. [[CrossRef](#)]
31. Cansiz, M.; Altinel, D.; Kurt, G.K. Efficiency in RF energy harvesting systems: A comprehensive review. *Energy* **2019**, *174*, 292–309. [[CrossRef](#)]
32. Selim, K.K.; Wu, S.; Saleeb, D.A. RF energy scavenging with a wide-range input power level. *IEEE Access* **2019**, *7*, 173450–173462. [[CrossRef](#)]
33. Mansour, M.M.; Kanaya, H. Compact and broadband RF rectifier with 1.5 octave bandwidth based on a simple pair of L-section matching network. *IEEE Microw. Wirel. Components Lett.* **2018**, *28*, 335–337. [[CrossRef](#)]
34. Muhammad, S.; Tiang, J.J.; Wong, S.K. Design of a Dual-Port Multi-Band Rectifier Circuit. In Proceedings of the 8th Global Conference on Engineering and Technology (CIETR-2020), Global Academy of Training and Research (GATR) Enterprise [002360364-P], Bangkok, Thailand, 12 December 2020 ; pp. 1–8.
35. Ellis, M.S.; Zhao, Z.; Wu, J.; Ding, X.; Nie, Z.; Liu, Q.H. A novel simple and compact microstrip-fed circularly polarized wide slot antenna with wide axial ratio bandwidth for C-band applications. *IEEE Trans. Antennas Propag.* **2016**, *64*, 1552–1555. [[CrossRef](#)]

36. Valenta, C.R.; Durgin, G.D. Harvesting wireless power: Survey of energy-harvester conversion efficiency in far-field, wireless power transfer systems. *IEEE Microw. Mag.* **2014**, *15*, 108–120.
37. Tesla, N. Apparatus for Transmitting Electrical Energy. U.S. Patent 1,119,732, 1 December 1914.
38. Midya, M.; Bhattacharjee, S.; Mitra, M. Triple-band dual-sense circularly polarised planar monopole antenna. *IET Microwaves Antennas Propag.* **2019**, *13*, 2020–2025. [[CrossRef](#)]
39. Ding, K.; Gao, C.; Yu, T.; Qu, D. Broadband C-shaped circularly polarized monopole antenna. *IEEE Trans. Antennas Propag.* **2014**, *63*, 785–790. [[CrossRef](#)]
40. Trainotti, V. Short medium frequency AM antennas. *IEEE Trans. Broadcast.* **2001**, *47*, 263–284. [[CrossRef](#)]
41. Sun, H.; Guo, Y.x.; He, M.; Zhong, Z. A dual-band rectenna using broadband Yagi antenna array for ambient RF power harvesting. *IEEE Antennas Wirel. Propag. Lett.* **2013**, *12*, 918–921. [[CrossRef](#)]
42. Li, L.; Zhou, Z.; Hong, J.; Wang, B.Z. Compact ultra-wideband printed monopole antenna. *Electron. Lett.* **2011**, *47*, 894–896. [[CrossRef](#)]
43. Pinuela, M.; Yates, D.; Mitcheson, P.; Lucyszyn, S. London RF survey for radiative ambient RF energy harvesters and efficient DC-load inductive power transfer. In Proceedings of the 2013 7th European Conference on Antennas and Propagation (EuCAP), Gothenburg, Sweden, 8–12 April 2013; pp. 2839–2843.
44. Darak, S.J.; Moy, C.; Palicot, J.; Louët, Y. Smart decision making policy for faster harvesting from ambient RF sources in wireless sensor nodes. In Proceedings of the 2016 International Symposium on Wireless Communication Systems (ISWCS), Poznan, Poland, 20–23 September 2016; pp. 148–152.
45. Bose, I.; Yan, S. The green potential of RFID projects: A case-based analysis. *IT Prof.* **2011**, *13*, 41–47. [[CrossRef](#)]
46. Bhatnagar, V.; Owende, P. Energy harvesting for assistive and mobile applications. *Energy Sci. Eng.* **2015**, *3*, 153–173. [[CrossRef](#)]
47. Lu, P.; Song, C.; Huang, K.M. Ultra-Wideband Rectenna Using Complementary Resonant Structure for Microwave Power Transmission and Energy Harvesting. *IEEE Trans. Microw. Theory Tech.* **2021**, *69*, 3452–3462. [[CrossRef](#)]
48. Kanaujia, B.K.; Singh, N.; Kumar, S. Background and Origin of the Rectenna. In *Rectenna: Wireless Energy Harvesting System*; Springer: Berlin/Heidelberg, Germany, 2021; pp. 21–48.
49. Abdelhalem, S.H.; Gudem, P.S.; Larson, L.E. An RF–DC converter with wide-dynamic-range input matching for power recovery applications. *IEEE Trans. Circuits Syst. II Express Briefs* **2013**, *60*, 336–340. [[CrossRef](#)]
50. Cai, X.; Wen, G.; Guo, Y. A Compact Rectenna with Flat-Top Angular Coverage for RF Energy Harvesting. *IEEE Antennas Wirel. Propag. Lett.* **2021**, *20*, 1307–1311. [[CrossRef](#)]
51. Muhammad, S.; Tiang, J.J.; Wong, S.K. Design of Wideband Circular Slot Antenna for RF Energy Harvesting System. In Proceedings of the DIFCON 2021: Digital Futures International Congress, Online, 21–23 June 2021; p. 74. Available online: <https://ieeexplore.ieee.org/abstract/document/6698485> (accessed on 9 February 2022).
52. Muhammad, S.; Jiat Tiang, J.; Kin Wong, S.; Iqbal, A.; Alibakhshikenari, M.; Limiti, E. Compact Rectifier Circuit Design for Harvesting GSM/900 Ambient Energy. *Electronics* **2020**, *9*, 1614. [[CrossRef](#)]
53. Cheney, M.; Uth, R. *Tesla, Master of Lightning*; Barnes & Noble Publishing: China, 1999.
54. Kraus, J.D. Heinrich Hertz-theorist and experimenter. *IEEE Trans. Microw. Theory Tech.* **1988**, *36*, 824–829. [[CrossRef](#)]
55. Chandravanshi, S.; Akhtar, M. Design of efficient rectifier using IDC and harmonic rejection filter in GSM/CDMA band for RF energy harvesting. *Microw. Opt. Technol. Lett.* **2017**, *59*, 681–686. [[CrossRef](#)]
56. Song, C.; Huang, Y.; Zhou, J.; Zhang, J.; Yuan, S.; Carter, P. A high-efficiency broadband rectenna for ambient wireless energy harvesting. *IEEE Trans. Antennas Propag.* **2015**, *63*, 3486–3495. [[CrossRef](#)]
57. Mohan, A.; Mondal, S. An Impedance Matching Strategy for Micro-Scale RF Energy Harvesting Systems. *IEEE Trans. Circuits Syst. II Express Briefs* **2020**, *68*, 1458–1462. [[CrossRef](#)]
58. Carlson, W.B. Margaret Cheney, Tesla: Man out of Time (Book Review). *Technol. Cult.* **1983**, *24*, 140. [[CrossRef](#)]
59. Muhammad, S.; Tiang, J.J.; Wong, S.K. Design of a broadband Long-Range RF-Rectifier Circuit for Harvesting Ambient Energy. In Proceedings of the DIFCON 2021: Digital Futures International Congress, Online, 21–23 June 2021; p. 82.
60. Luo, Y.; Chin, K.W. Learning to Charge RF-Energy Harvesting Devices in WiFi Networks. *IEEE Syst. J.* **2021**, *15*, 5516–5525. [[CrossRef](#)]
61. Sarker, M.R.; Saad, M.H.M.; Olazagoitia, J.L.; Vinolas, J. Review of Power Converter Impact of Electromagnetic Energy Harvesting Circuits and Devices for Autonomous Sensor Applications. *Electronics* **2021**, *10*, 1108. [[CrossRef](#)]
62. Maxwell, J.C. VIII. A dynamical theory of the electromagnetic field. *Philos. Trans. R. Soc. Lond.* **1865**, 459–512.
63. Tang, X.; Xie, G.; Cui, Y. Self-sustainable Long Range Backscattering Communication Using RF Energy Harvesting. *IEEE Internet Things J.* **2021**, *8*, 13737–13749. [[CrossRef](#)]
64. Inbaraj, D.; Kailasam, M.; Sankararajan, R. Statistical analysis on ambient RF energy harvesting for low-power wireless applications. *Int. J. Commun. Syst.* **2018**, *31*, e3538. [[CrossRef](#)]
65. Le, G.; Nguyen, N.; Au, N.D.; Seo, C. A Broadband High-Efficiency Rectifier for Mid-field Wireless Power Transfer. *IEEE Microw. Wirel. Components Lett.* **2021**, *31*, 913–916. [[CrossRef](#)]
66. Visser, H.J.; Reniers, A.C.; Theeuwes, J.A. Ambient RF energy scavenging: GSM and WLAN power density measurements. In Proceedings of the 2008 38th European Microwave Conference, Amsterdam, The Netherlands, 27–31 October 2008; pp. 721–724.

67. Le, M.T.; Vu, H.S.; Truong, T.; Vu, H.T.; Nguyen, Q.C. Circularly polarized meandered-loop antenna for ambient RF energy harvesting system. In Proceedings of the 2020 IEEE Eighth International Conference on Communications and Electronics (ICCE), Phu Quoc Island, Vietnam, 13–15 January 2021; pp. 225–229.
68. Yang, X.X.; Jiang, C.; Elsherbeni, A.Z.; Yang, F.; Wang, Y.Q. A novel compact printed rectenna for data communication systems. *IEEE Trans. Antennas Propag.* **2013**, *61*, 2532–2539. [[CrossRef](#)]
69. Bayat, P.; Baghrmian, A. A novel self-tuning type-2 fuzzy maximum power point tracking technique for efficiency enhancement of fuel cell based battery chargers. *Int. J. Hydrogen Energy* **2020**, *45*, 23275–23293. [[CrossRef](#)]
70. Lin, C.H.; Zhuang, Y.D.; Tsai, D.G.; Wei, H.J.; Liu, T.Y. Performance Enhancement of Vanadium Redox Flow Battery by Treated Carbon Felt Electrodes of Polyacrylonitrile using Atmospheric Pressure Plasma. *Polymers* **2020**, *12*, 1372. [[CrossRef](#)] [[PubMed](#)]
71. Wang, G.; Gao, Q.; Yan, Y.; Zhang, Y. Transient process optimization of battery cooling on heat transfer enhancement structure. *Appl. Therm. Eng.* **2021**, *182*, 115897. [[CrossRef](#)]
72. Huang, Y.; Shinohara, N.; Toromura, H. A wideband rectenna for 2.4 GHz-band RF energy harvesting. In Proceedings of the 2016 IEEE Wireless Power Transfer Conference (WPTC), Aveiro, Portugal, 5–6 May 2016; pp. 1–3.
73. Ouyang, P.; Jin, C.; Xu, G.; Yang, X.; Kong, K.; Liu, B.; Dan, J.; Chen, J.; Yue, Z.; Li, X.; et al. Lithium ion batteries with enhanced electrochemical performance by using carbon-coated SiOx/Ag composites as anode material. *Ceram. Int.* **2021**, *47*, 1086–1094. [[CrossRef](#)]
74. Pardue, C.A.; Bellaredj, M.L.F.; Torun, H.M.; Swaminathan, M.; Kohl, P.; Davis, A.K. RF wireless power transfer using integrated inductor. *IEEE Trans. Components Packag. Manuf. Technol.* **2018**, *9*, 913–920. [[CrossRef](#)]
75. Muhammad, S.; Jiat Tiang, J.; Kin Wong, S.; Jamel, N.; Iqbal, A. Design of a Five-Band Dual-Port Rectenna for RF Energy Harvesting. *Comput. Mater. Contin.* **2021**, *69*, 487–501. [[CrossRef](#)]
76. Muhammad, S.; Tiang, J.J.; Wong, S.K.; Smida, A.; Ghayoula, R.; Iqbal, A. A Dual-band Ambient Energy Harvesting Rectenna Design for Wireless Power Communications. *IEEE Access* **2021**, *9*, 99944–99953. [[CrossRef](#)]
77. Harouni, Z.; Osman, L.; Gharsallah, A. Efficient 2.45 GHz CPW patch antenna including harmonic rejecting device for wireless power transmission. In Proceedings of the Eighth International Multi-Conference on Systems, Signals & Devices, Sousse, Tunisia, 22–25 March 2011; pp. 1–3.
78. Song, C.; Huang, Y.; Zhou, J.; Carter, P. Improved ultrawideband rectennas using hybrid resistance compression technique. *IEEE Trans. Antennas Propag.* **2017**, *65*, 2057–2062. [[CrossRef](#)]
79. Brown, W.; Mims, J.; Heenan, N. An experimental microwave-powered helicopter. In Proceedings of the 1958 IRE International Convention Record, New York, NY, USA, 21–25 March 1966; Volume 13, pp. 225–235.
80. Glaser, P.E. Power from the sun: Its future. *Science* **1968**, *162*, 857–861. [[CrossRef](#)] [[PubMed](#)]
81. Hossain, M.M.; Prybutok, V.R. Consumer acceptance of RFID technology: An exploratory study. *IEEE Trans. Eng. Manag.* **2008**, *55*, 316–328. [[CrossRef](#)]
82. Tissier, J.; Latrach, M. A 900/1800 MHz dual-band high-efficiency rectenna. *Microw. Opt. Technol. Lett.* **2019**, *61*, 1278–1283. [[CrossRef](#)]
83. Moradi, E.; Sydänheimo, L.; Bova, G.S.; Ukkonen, L. Measurement of wireless power transfer to deep-tissue RFID-based implants using wireless repeater node. *IEEE Antennas Wirel. Propag. Lett.* **2017**, *16*, 2171–2174. [[CrossRef](#)]
84. Pandey, R.; Shankhwar, A.K.; Singh, A. An improved conversion efficiency of 1.975 to 4.744 GHz rectenna for wireless sensor applications. *Prog. Electromagn. Res. C* **2021**, *109*, 217–225. [[CrossRef](#)]
85. Abdi, A.; Aliakbarian, H. A miniaturized UHF-band rectenna for power transmission to deep-body implantable devices. *IEEE J. Transl. Eng. Health Med.* **2019**, *7*, 1–11. [[CrossRef](#)] [[PubMed](#)]
86. Lui, K.; Murphy, O.; Toumazou, C. A wearable wideband circularly polarized textile antenna for effective power transmission on a wirelessly-powered sensor platform. *IEEE Trans. Antennas Propag.* **2013**, *61*, 3873–3876. [[CrossRef](#)]
87. Lu, X.; Wang, P.; Niyato, D.; Kim, D.I.; Han, Z. Wireless networks with RF energy harvesting: A contemporary survey. *IEEE Commun. Surv. Tutorials* **2014**, *17*, 757–789. [[CrossRef](#)]
88. Ma, Z.; Vandenbosch, G.A. Wideband harmonic rejection filtenna for wireless power transfer. *IEEE Trans. Antennas Propag.* **2013**, *62*, 371–377. [[CrossRef](#)]
89. Pardue, C.A.; Bellaredj, M.L.F.; Davis, A.K.; Swaminathan, M.; Kohl, P.; Fujii, T.; Nakazawa, S. Design and characterization of inductors for self-powered IoT edge devices. *IEEE Trans. Components Packag. Manuf. Technol.* **2018**, *8*, 1263–1271. [[CrossRef](#)]
90. Chandrasekaran, K.T.; Agarwal, K.; Nasimuddin; Alphones, A.; Mitra, R.; Karim, M.F.; Compact Dual-Band Metamaterial-Based High-Efficiency Rectenna: An Application for Ambient Electromagnetic Energy Harvesting. *IEEE Antennas Propag. Mag.* **2020**, *62*, 18–29. [[CrossRef](#)]
91. Song, C.; López-Yela, A.; Huang, Y.; Segovia-Vargas, D.; Zhuang, Y.; Wang, Y.; Zhou, J. A novel quartz clock with integrated wireless energy harvesting and sensing functions. *IEEE Trans. Ind. Electron.* **2018**, *66*, 4042–4053. [[CrossRef](#)]
92. Wagih, M.; Weddell, A.S.; Beeby, S. Rectennas for radio-frequency energy harvesting and wireless power transfer: A review of antenna design [antenna applications corner]. *IEEE Antennas Propag. Mag.* **2020**, *62*, 95–107. [[CrossRef](#)]
93. Sanou, B. ICT Facts and Figures. 2013. Available online: <https://eldis.org/document/A65910> (accessed on 8 June 2021).
94. Niotaki, K.; Kim, S.; Jeong, S.; Collado, A.; Georgiadis, A.; Tentzeris, M.M. A compact dual-band rectenna using slot-loaded dual band folded dipole antenna. *IEEE Antennas Wirel. Propag. Lett.* **2013**, *12*, 1634–1637. [[CrossRef](#)]

95. Liu, J.; Xue, Q.; Wong, H.; Lai, H.W.; Long, Y. Design and analysis of a low-profile and broadband microstrip monopolar patch antenna. *IEEE Trans. Antennas Propag.* **2012**, *61*, 11–18. [CrossRef]
96. Mishra, D.; De, S.; Jana, S.; Basagni, S.; Chowdhury, K.; Heinzelman, W. Smart RF energy harvesting communications: Challenges and opportunities. *IEEE Commun. Mag.* **2015**, *53*, 70–78. [CrossRef]
97. Boaventura, A.; Belo, D.; Fernandes, R.; Collado, A.; Georgiadis, A.; Carvalho, N.B. Boosting the efficiency: Unconventional waveform design for efficient wireless power transfer. *IEEE Microw. Mag.* **2015**, *16*, 87–96. [CrossRef]
98. Collado, A.; Georgiadis, A. Conformal hybrid solar and electromagnetic (EM) energy harvesting rectenna. *IEEE Trans. Circuits Syst. I Regul. Pap.* **2013**, *60*, 2225–2234. [CrossRef]
99. James, M.C. II. A dynamical theory of the electromagnetic field. *Proc. R. Soc. Lond.* **1864**, 531–536. [CrossRef]
100. Surender, D.; Khan, T.; Talukdar, F.A.; De, A.; Antar, Y.M.; Freundorfer, A.P. Key Components of Rectenna System: A Comprehensive Survey. *IETE J. Res.* **2020**, 1–27. [CrossRef]
101. Vullers, R.J.; Van Schaijk, R.; Visser, H.J.; Penders, J.; Van Hoof, C. Energy harvesting for autonomous wireless sensor networks. *IEEE Solid-State Circuits Mag.* **2010**, *2*, 29–38. [CrossRef]
102. ABRACON. Whip Antenna Datasheet PDF. 2018. Available online: <http://www.farnell.com/datasheets/2647385.pdf> (accessed on 5 July 2019).
103. Du, Z.X.; Bo, S.F.; Cao, Y.F.; Ou, J.H.; Zhang, X.Y. Broadband Circularly Polarized Rectenna with Wide Dynamic-Power-Range for Efficient Wireless Power Transfer. *IEEE Access* **2020**, *8*, 80561–80571. [CrossRef]
104. Marinčić, A.; Civrić, Z.; Milovanović, B. Nikola Tesla's contributions to radio developments. *Serbian J. Electr. Eng.* **2006**, *3*, 131–148. [CrossRef]
105. Song, N.S.; Chin, K.L.; Liang, D.B.B.; Anyi, M. Design of broadband dual-frequency microstrip patch antenna with modified sierpinski fractal geometry. In Proceedings of the 2006 10th IEEE Singapore International Conference on Communication Systems, Singapore, 30 October–1 November 2006; pp. 1–5.
106. Dafallaa, W.A. Wideband Antenna Design for Frequency Band Between 2.4 and 11 GHz. Ph.D. Thesis, Universiti Teknologi Malaysia, Skudai, Malaysia, 2010.
107. Balanis, C.A. *Antenna Theory: Analysis and Design*; John Wiley & Sons: Hoboken, NJ, USA, 2015.
108. Pozar, D.M. *Microwave Engineering*; Wiley: Hoboken, NJ, USA, 2012.
109. Adam, I.; M. Yasin, M.N.; Soh, P.J.; Kamardin, K.; Jamlos, M.F.; Lago, H.; Razalli, M.S. A simple wideband electromagnetically fed circular polarized antenna for energy harvesting. *Microw. Opt. Technol. Lett.* **2017**, *59*, 2390–2397. [CrossRef]
110. Awais, Q.; Jin, Y.; Chattha, H.T.; Jamil, M.; Qiang, H.; Khawaja, B.A. A compact rectenna system with high conversion efficiency for wireless energy harvesting. *IEEE Access* **2018**, *6*, 35857–35866. [CrossRef]
111. Dias, L.F.R.; Boaventua, A.; de Carvalho, N.B. RF-DC converter efficiency optimization using source-pull techniques. In Proceedings of the 2014 International Workshop on Integrated Nonlinear Microwave and Millimetre-Wave Circuits (INMMiC), Leuven, Belgium, 2–4 April 2014; pp. 1–3.
112. Zhang, R.; Ho, C.K. MIMO broadcasting for simultaneous wireless information and power transfer. *IEEE Trans. Wirel. Commun.* **2013**, *12*, 1989–2001. [CrossRef]
113. Mansour, M.M.; Kanaya, H. Novel L-slot matching circuit integrated with circularly polarized rectenna for wireless energy harvesting. *Electronics* **2019**, *8*, 651. [CrossRef]
114. Muhammad, S.; Ya'u, I.; Abubakar, A.; Yaro, A.S. Design of single feed dual-band millimeter wave antenna for future 5G wireless applications. *Sci. World J.* **2019**, *14*, 84–87.
115. Fujimoto, T.; Jono, K. Wideband rectangular printed monopole antenna for circular polarisation. *IET Microwaves Antennas Propag.* **2014**, *8*, 649–656. [CrossRef]
116. Pakkathillam, J.K.; Kanagasabai, M. Circularly polarized broadband antenna deploying fractal slot geometry. *IEEE Antennas Wirel. Propag. Lett.* **2015**, *14*, 1286–1289. [CrossRef]
117. Soltani, S.; Azarmanesh, M.; Lotfi, P.; Dadashzadeh, G. Two novel very small monopole antennas having frequency band notch function using DGS for UWB application. *AEU-Int. J. Electron. Commun.* **2011**, *65*, 87–94. [CrossRef]
118. Chang, K.M.; Lin, R.J.; Deng, I.C.; Chen, J.B.; Xiang, K.Q.; Rong, C.J. A novel design of a CPW-fed square slot antenna with broadband circular polarization. *Microw. Opt. Technol. Lett.* **2006**, *48*, 2456–2459. [CrossRef]
119. Sabran, M.L.; Rahim, S.K.A.; Soh, P.J.; Leow, C.Y.; Vandenbosch, G. A simple electromagnetically fed circularly-polarized circular microstrip antenna. *Appl. Comput. Electromagn. Soc. J.* **2015**, *30*, 1180–1187.
120. Lee, H.; Lee, S.R.; Lee, K.J.; Kong, H.B.; Lee, I. Transmit beamforming techniques for wireless information and power transfer in MISO interference channels. In Proceedings of the 2015 IEEE Global Communications Conference (GLOBECOM), San Diego, CA, USA, 6–10 December 2015; pp. 1–6.
121. Chen, Y.S.; You, J.W. A scalable and multidirectional rectenna system for RF energy harvesting. *IEEE Trans. Components Packag. Manuf. Technol.* **2018**, *8*, 2060–2072. [CrossRef]
122. Panahi, A.; Bao, X.; Ruvio, G.; Ammann, M. A printed triangular monopole with wideband circular polarization. *IEEE Trans. Antennas Propag.* **2014**, *63*, 415–418. [CrossRef]
123. Ahmed, S.; Zakaria, Z.; Husain, M.; Ibrahim, I.; Alhegazi, A. Efficient feeding geometries for rectenna design at 2.45 GHz. *Electron. Lett.* **2017**, *53*, 1585–1587. [CrossRef]

124. Zainol, N.; Zakaria, Z.; Abu, M.; Mohamed Yunus, M. A 2.45 GHz harmonic suppression rectangular patch antenna with circular polarization for wireless power transfer application. *IETE J. Res.* **2018**, *64*, 310–316. [[CrossRef](#)]
125. Liu, Y.; Huang, K.; Yang, Y.; Zhang, B. A low-profile lightweight circularly polarized rectenna array based on coplanar waveguide. *IEEE Antennas Wirel. Propag. Lett.* **2018**, *17*, 1659–1663. [[CrossRef](#)]
126. Masius, A.A.; Wong, Y.C.; Lau, K.T. Miniature high gain slot-fed rectangular dielectric resonator antenna for IoT RF energy harvesting. *AEU-Int. J. Electron. Commun.* **2018**, *85*, 39–46. [[CrossRef](#)]
127. Sun, W.J.; Yang, W.W.; Chu, P.; Chen, J.X. A wideband stacked dielectric resonator antenna for 5G applications. *Int. J. RF Microw. Comput.-Aided Eng.* **2019**, *29*, e21897. [[CrossRef](#)]
128. Sun, H. An enhanced rectenna using differentially-fed rectifier for wireless power transmission. *IEEE Antennas Wirel. Propag. Lett.* **2015**, *15*, 32–35. [[CrossRef](#)]
129. McSpadden, J.O.; Fan, L.; Chang, K. Design and experiments of a high-conversion-efficiency 5.8-GHz rectenna. *IEEE Trans. Microw. Theory Tech.* **1998**, *46*, 2053–2060. [[CrossRef](#)]
130. Yu, C.; Tan, F.; Liu, C. A C-band microwave rectenna using aperture-coupled antenna array and novel Class-F rectifier with cavity. *J. Electromagn. Waves Appl.* **2015**, *29*, 977–991. [[CrossRef](#)]
131. Singh, M.; Agrawal, S.; Parihar, M.S. Design of a rectenna system for GSM-900 band using novel broadside  $2 \times 1$  array antenna. *J. Eng.* **2017**, *2017*, 232–236. [[CrossRef](#)]
132. Shen, S.; Zhang, Y.; Chiu, C.Y.; Murch, R. Directional Multiport Ambient RF Energy Harvesting System for the Internet of Things. *IEEE Internet Things J.* **2020**, *8*, 5850–5865. [[CrossRef](#)]
133. Ladan, S.; Ghassemi, N.; Ghiotto, A.; Wu, K. Highly efficient compact rectenna for wireless energy harvesting application. *IEEE Microw. Mag.* **2013**, *14*, 117–122. [[CrossRef](#)]
134. Wang, M.; Yang, L.; Fan, Y.; Shen, M.; Li, Y.; Shi, Y. A compact omnidirectional dual-circular rectenna for 2.45 GHz wireless power transfer. *Int. J. RF Microw. Comput.-Aided Eng.* **2019**, *29*, e21625. [[CrossRef](#)]
135. Huang, F.J.; Lee, C.M.; Chang, C.L.; Chen, L.K.; Yo, T.C.; Luo, C.H. Rectenna application of miniaturized implantable antenna design for triple-band biotelemetry communication. *IEEE Trans. Antennas Propag.* **2011**, *59*, 2646–2653. [[CrossRef](#)]
136. Kuhn, V.; Lahuec, C.; Seguin, F.; Person, C. A multi-band stacked RF energy harvester with RF-to-DC efficiency up to 84%. *IEEE Trans. Microw. Theory Tech.* **2015**, *63*, 1768–1778. [[CrossRef](#)]
137. Agrawal, S.; Parihar, M.S.; Kondekar, P.N. A dual-band rectenna using broadband DRA loaded with slot. *Int. J. Microw. Wirel. Technol.* **2018**, *10*, 59. [[CrossRef](#)]
138. Zeng, M.; Li, Z.; Andrenko, A.S.; Zeng, Y.; Tan, H.Z. A compact dual-band rectenna for GSM900 and GSM1800 energy harvesting. *Int. J. Antennas Propag.* **2018**, *2018*, 4781465. [[CrossRef](#)]
139. Shen, S.; Chiu, C.Y.; Murch, R.D. A dual-port triple-band L-probe microstrip patch rectenna for ambient RF energy harvesting. *IEEE Antennas Wirel. Propag. Lett.* **2017**, *16*, 3071–3074. [[CrossRef](#)]
140. Liu, J.; Zhang, X.Y.; Yang, C.L. Analysis and design of dual-band rectifier using novel matching network. *IEEE Trans. Circuits Syst. II Express Briefs* **2017**, *65*, 431–435. [[CrossRef](#)]
141. Zhu, L.; Zhang, J.; Han, W.; Xu, L.; Bai, X. A novel RF energy harvesting cube based on air dielectric antenna arrays. *Int. J. RF Microw. Comput.-Aided Eng.* **2019**, *29*, e21636. [[CrossRef](#)]
142. Sun, H.; Guo, Y.x.; He, M.; Zhong, Z. Design of a high-efficiency 2.45-GHz rectenna for low-input-power energy harvesting. *IEEE Antennas Wirel. Propag. Lett.* **2012**, *11*, 929–932.
143. Hassan, N.; Zakaria, Z.; Sam, W.Y.; Hanapiah, I.N.M.; Mohamad, A.N.; Roslan, A.F.; Ahmad, B.H.; Ismail, M.K.; Abd Aziz, M.Z.A. Design of dual-band microstrip patch antenna with right-angle triangular aperture slot for energy transfer application. *Int. J. RF Microw. Comput.-Aided Eng.* **2019**, *29*, e21666. [[CrossRef](#)]
144. Chandravanshi, S.; Sarma, S.S.; Akhtar, M.J. Design of triple band differential rectenna for RF energy harvesting. *IEEE Trans. Antennas Propag.* **2018**, *66*, 2716–2726. [[CrossRef](#)]
145. Yusop, M.; Rahim, M.; Ismail, M.; Wahid, A. Circular polarization fractal koch microstrip patch antenna using single-fed EM coupled ring resonators. In Proceedings of the 2010 IEEE Asia-Pacific Conference on Applied Electromagnetics (APACE), Port Dickson, Malaysia, 9–11 November 2010; pp. 1–4.
146. Mohd Noor, F.S.; Zakaria, Z.; Lago, H.; Meor Said, M.A. Dual-band aperture-coupled rectenna for radio frequency energy harvesting. *Int. J. RF Microw. Comput.-Aided Eng.* **2019**, *29*, e21651. [[CrossRef](#)]
147. Lu, J.H.; Wang, S.F. Planar broadband circularly polarized antenna with square slot for UHF RFID reader. *IEEE Trans. Antennas Propag.* **2012**, *61*, 45–53. [[CrossRef](#)]
148. Nie, M.J.; Yang, X.X.; Tan, G.N.; Han, B. A compact 2.45-GHz broadband rectenna using grounded coplanar waveguide. *IEEE Antennas Wirel. Propag. Lett.* **2015**, *14*, 986–989. [[CrossRef](#)]
149. Agrawal, S.; Gupta, R.D.; Parihar, M.S.; Kondekar, P.N. A wideband high gain dielectric resonator antenna for RF energy harvesting application. *AEU-Int. J. Electron. Commun.* **2017**, *78*, 24–31. [[CrossRef](#)]
150. Agrawal, S.; Parihar, M.S.; Kondekar, P. Broadband rectenna for radio frequency energy harvesting application. *IETE J. Res.* **2018**, *64*, 347–353. [[CrossRef](#)]
151. Timotheou, S.; Zheng, G.; Masouros, C.; Krikidis, I. Exploiting constructive interference for simultaneous wireless information and power transfer in multiuser downlink systems. *IEEE J. Sel. Areas Commun.* **2016**, *34*, 1772–1784. [[CrossRef](#)]

152. Muhammad, S.; Tiang, J.J.; Wong, S.K.; Smida, A.; Waly, M.I.; Iqbal, A. Efficient Quad-band RF Energy Harvesting Rectifier for Wireless Power Communications. *AEU-Int. J. Electron. Commun.* **2021**, *139*, 153927. [CrossRef]
153. Falkenstein, E.; Roberg, M.; Popovic, Z. Low-power wireless power delivery. *IEEE Trans. Microw. Theory Tech.* **2012**, *60*, 2277–2286. [CrossRef]
154. Verma, M.K.; Kanaujia, B.K.; Saini, J.P.; Singh, P. A compact multi-slots loaded gap coupled CP antenna with DGS for WLAN/WiMAX applications. *Int. J. RF Microw. Comput.-Aided Eng.* **2020**, *30*, e22431. [CrossRef]
155. Rezaeieh, S.A.; Abbosh, A.; Antoniadis, M.A. Compact CPW-fed planar monopole antenna with wide circular polarization bandwidth. *IEEE Antennas Wirel. Propag. Lett.* **2013**, *12*, 1295–1298. [CrossRef]
156. Jan, J.Y.; Pan, C.Y.; Chiu, K.Y.; Chen, H.M. Broadband CPW-fed circularly-polarized slot antenna with an open slot. *IEEE Trans. Antennas Propag.* **2012**, *61*, 1418–1422. [CrossRef]
157. Bai, X.; Zhang, J.w.; Xu, L.j. A broadband CPW fractal antenna for RF energy harvesting. In Proceedings of the 2017 International Applied Computational Electromagnetics Society Symposium (ACES), Suzhou, China, 1–4 August 2017; pp. 1–2.
158. Saranya, N.; Kesavamurthy, T. Design and performance analysis of broadband rectenna for an efficient RF energy harvesting application. *Int. J. RF Microw. Comput.-Aided Eng.* **2019**, *29*, e21628. [CrossRef]
159. Kumar, H.; Arrawatia, M.; Kumar, G. Broadband planar log-periodic dipole array antenna based RF-energy harvesting system. *IETE J. Res.* **2019**, *65*, 39–43. [CrossRef]
160. Shi, Y.; Fan, Y.; Li, Y.; Yang, L.; Wang, M. An efficient broadband slotted rectenna for wireless power transfer at LTE band. *IEEE Trans. Antennas Propag.* **2018**, *67*, 814–822. [CrossRef]
161. Lin, Z.; Lin, M.; Zhu, W.P.; Wang, J.B.; Cheng, J. Robust secure beamforming for wireless powered cognitive satellite-terrestrial networks. *IEEE Trans. Cogn. Commun. Netw.* **2020**, *7*, 567–580. [CrossRef]
162. Al-Zoubi, A.; Yang, F.; Kishk, A. A broadband center-fed circular patch-ring antenna with a monopole like radiation pattern. *IEEE Trans. Antennas Propag.* **2009**, *57*, 789–792. [CrossRef]
163. Mavrikis, D. Small Cell Market Status December 2012. 2012. Available online: <https://the-mobile-network.com/2021/04/small-cells-market-update-2021/> (accessed on 7 September 2021).
164. Palazzi, V.; Del Prete, M.; Fantuzzi, M. Scavenging for energy: A rectenna design for wireless energy harvesting in UHF mobile telephony bands. *IEEE Microw. Mag.* **2016**, *18*, 91–99. [CrossRef]
165. Ntougias, K.; Krikidis, I.; Papageorgiou, G.K.; Sellathurai, M. Hybrid Precoding for MISO Broadcasting SWIPT Systems: A Stochastic Optimization Approach. In Proceedings of the 2020 IEEE 31st Annual International Symposium on Personal, Indoor and Mobile Radio Communications, London, UK, 31 August–3 September 2020; pp. 1–7.
166. Yang, H.; Xia, X.; Li, J.; Zhu, P.; You, X. Joint Transceiver Design for Network-Assisted Full-Duplex Systems with SWIPT. *IEEE Syst. J.* **2021**, 1–11. [CrossRef]
167. Muhammad, S.; Yaro, A.S.; Alhassan, I.B. Wide-band 4G Mobile Device Planar Antenna Using Couple Feeding Technique. *ATBU J. Sci. Technol. Educ.* **2018**, *5*, 107–116.
168. Zhang, L.; Jiao, Y.C.; Ding, Y.; Chen, B.; Weng, Z.B. CPW-fed broadband circularly polarized planar monopole antenna with improved ground-plane structure. *IEEE Trans. Antennas Propag.* **2013**, *61*, 4824–4828. [CrossRef]
169. Palazzi, V.; Hester, J.; Bitto, J.; Alimenti, F.; Kalialakis, C.; Collado, A.; Mezzanotte, P.; Georgiadis, A.; Roselli, L.; Tentzeris, M.M. A novel ultra-lightweight multiband rectenna on paper for RF energy harvesting in the next generation LTE bands. *IEEE Trans. Microw. Theory Tech.* **2017**, *66*, 366–379. [CrossRef]
170. Cui, L.; Wu, W.; Fang, D.G. Wideband circular patch antenna with conical radiation pattern. *IEEE Antennas Wirel. Propag. Lett.* **2014**, *14*, 458–461. [CrossRef]
171. Marian, V.; Vollaie, C.; Verdier, J.; Allard, B. Potentials of an adaptive rectenna circuit. *IEEE Antennas Wirel. Propag. Lett.* **2011**, *10*, 1393–1396. [CrossRef]
172. Lopez, A.R. Review of narrowband impedance-matching limitations. *IEEE Antennas Propag. Mag.* **2004**, *46*, 88–90. [CrossRef]
173. Alfred, L.R. More on narrowband impedance-matching limitations. *IEEE Antennas Propag. Mag.* **2004**, *46*, 102.
174. Frenzel, L. Back to basics: Impedance matching (part 1). *Electron. Des.* **2011**, *24*. Available online: <https://www.electronicdesign.com/technologies/communications/article/21796367/back-to-basics-impedance-matching-part-1> (accessed on 15 July 2020).
175. Shinohara, N.; Matsumoto, H. Experimental study of large rectenna array for microwave energy transmission. *IEEE Trans. Microw. Theory Tech.* **1998**, *46*, 261–268. [CrossRef]
176. Yang, S.; Lee, K.F.; Kishk, A.; Luk, K.M. Design and study of wideband single feed circularly polarized microstrip antennas. *Prog. Electromagn. Res.* **2008**, *80*, 45–61. [CrossRef]
177. Choi, J.; Chung, K.; Roh, Y. Parametric analysis of a band-rejection antenna for UWB application. *Microw. Opt. Technol. Lett.* **2005**, *47*, 287–290. [CrossRef]
178. Liang, W.L.; Jiao, Y.C.; Zhang, L.; Ni, T. Wideband single-feed circularly polarized antenna. *Prog. Electromagn. Res. Lett.* **2015**, *54*, 93–99. [CrossRef]
179. Bolos, F.; Belo, D.; Georgiadis, A. A UHF rectifier with one octave bandwidth based on a non-uniform transmission line. In Proceedings of the 2016 IEEE MTT-S International Microwave Symposium (IMS), San Francisco, CA, USA, 22–27 May 2016; pp. 1–3.
180. Soyata, T.; Copeland, L.; Heinzelman, W. RF energy harvesting for embedded systems: A survey of tradeoffs and methodology. *IEEE Circuits Syst. Mag.* **2016**, *16*, 22–57. [CrossRef]

181. Du, Z.X.; Zhang, X.Y. High-efficiency single-and dual-band rectifiers using a complex impedance compression network for wireless power transfer. *IEEE Trans. Ind. Electron.* **2017**, *65*, 5012–5022. [[CrossRef](#)]
182. Heydari Nasab, S.; Asefi, M.; Albasha, L.; Qaddoumi, N. Investigation of RF signal energy harvesting. *Act. Passiv. Electron. Components* **2010**, *2010*, 591640. [[CrossRef](#)]
183. Shen, S.; Chiu, C.Y.; Murch, R.D. Multiport pixel rectenna for ambient RF energy harvesting. *IEEE Trans. Antennas Propag.* **2017**, *66*, 644–656. [[CrossRef](#)]
184. Shanpu, S.; Zhang, Y.; Chiu, C.Y.; Murch, R. An ambient RF energy harvesting system where the number of antenna ports is dependent on frequency. *IEEE Trans. Microw. Theory Tech.* **2019**, *67*, 3821–3832.
185. Mansour, M.M.; Kanaya, H. High-efficient broadband CPW RF rectifier for wireless energy harvesting. *IEEE Microw. Wirel. Components Lett.* **2019**, *29*, 288–290. [[CrossRef](#)]
186. Adam, I.; M. Yasin, M.N.; A. Rahim, H.; Soh, P.J.; Abdulmalek, M.F. A compact dual-band rectenna for ambient RF energy harvesting. *Microw. Opt. Technol. Lett.* **2018**, *60*, 2740–2748. [[CrossRef](#)]
187. Partal, H.P.; Belen, M.A.; Partal, S.Z. Design and realization of an ultra-low power sensing RF energy harvesting module with its RF and DC sub-components. *Int. J. RF Microw. Comput.-Aided Eng.* **2019**, *29*, e21622. [[CrossRef](#)]
188. Hertz, H. *Electric Waves*; English Translation by JONES, DE, 1893. Available online: <https://www.abebooks.com/Electric-Waves-Authorised-English-Translation-Jones/30774333566/bd> (accessed on 10 February 2020).
189. Le, T.; Mayaram, K.; Fiez, T. Efficient far-field radio frequency energy harvesting for passively powered sensor networks. *IEEE J. Solid-State Circuits* **2008**, *43*, 1287–1302. [[CrossRef](#)]
190. Saffari, P.; Basaligheh, A.; Moez, K. An rf-to-dc rectifier with high efficiency over wide input power range for rf energy harvesting applications. *IEEE Trans. Circuits Syst. I Regul. Pap.* **2019**, *66*, 4862–4875. [[CrossRef](#)]
191. Yoo, T.W.; Chang, K. Theoretical and experimental development of 10 and 35 GHz rectennas. *IEEE Trans. Microw. Theory Tech.* **1992**, *40*, 1259–1266. [[CrossRef](#)]
192. Behera, B.R.; Meher, P.R.; Mishra, S.K. Microwave antennas—An intrinsic part of RF energy harvesting systems: A contingent study about its design methodologies and state-of-art technologies in current scenario. *Int. J. RF Microw. Comput.-Aided Eng.* **2020**, *30*, e22148. [[CrossRef](#)]
193. Md Din, N.; Chakrabarty, C.K.; Bin Ismail, A.; Devi, K.K.A.; Chen, W.Y. Design of RF energy harvesting system for energizing low power devices. *Prog. Electromagn. Res.* **2012**, *132*, 49–69. [[CrossRef](#)]
194. Marian, V.; Menudier, C.; Thevenot, M.; Vollaie, C.; Verdier, J.; Allard, B. Efficient design of rectifying antennas for low power detection. In Proceedings of the 2011 IEEE MTT-S International Microwave Symposium, Baltimore, MD, USA, 5–10 June 2011; pp. 1–4.
195. Skaik, T. A quad-band rectifier design with improved matching bandwidth for RF energy harvesting applications. In Proceedings of the 2017 International Conference on Promising Electronic Technologies (ICPET), Deir El-Balah, Palestine, 16–17 October 2017; pp. 82–86.
196. Park, J.Y.; Han, S.M.; Itoh. A rectenna design with harmonic-rejecting circular-sector antenna. *IEEE Antennas Wirel. Propag. Lett.* **2004**, *3*, 52–54. [[CrossRef](#)]
197. Alex-Amor, A.; Palomares-Caballero, Á.; Fernández-González, J.M.; Padilla, P.; Marcos, D.; Sierra-Castañer, M.; Esteban, J. RF energy harvesting system based on an archimedean spiral antenna for low-power sensor applications. *Sensors* **2019**, *19*, 1318. [[CrossRef](#)] [[PubMed](#)]
198. Elhebeary, M.R.; Ibrahim, M.A.; Aboudina, M.M.; Mohieldin, A.N. Dual-source self-start high-efficiency microscale smart energy harvesting system for IoT. *IEEE Trans. Ind. Electron.* **2017**, *65*, 342–351. [[CrossRef](#)]
199. Eshtiaghi, R.; Zaker, R.; Nouronia, J.; Ghobadi, C. UWB semi-elliptical printed monopole antenna with subband rejection filter. *AEU-Int. J. Electron. Commun.* **2010**, *64*, 133–141. [[CrossRef](#)]
200. Ltd, N.D.K.C. *Dengyo Rectennas Tokyo, Japan, 2012*. Available online: <https://techcrunch.com/2011/08/03/harvesting-energy-from-radio-signals-two-new-devices-from-japan-video/> (accessed on 2 May 2018).
201. Agrawal, S.; Parihar, M.S.; Kondekar, P.N. Exact Performance Evaluation of RF Energy Harvesting with Different Circuit's Elements. *IETE Tech. Rev.* **2018**, *35*, 514–522. [[CrossRef](#)]
202. Chang, Y.; Zhang, P.; Wang, L. Highly efficient differential rectenna for RF energy harvesting. *Microw. Opt. Technol. Lett.* **2019**, *61*, 2662–2668. [[CrossRef](#)]
203. Nimo, A.; Grgic, D.; Reindl, L.M. Impedance optimization of wireless electromagnetic energy harvesters for maximum output efficiency at  $\mu\text{W}$  input power. In Proceedings of the Active and Passive Smart Structures and Integrated Systems 2012, San Diego, CA, USA, 12–15 March 2012; Volume 8341, p. 83410W. [[CrossRef](#)]
204. Ungan, T.; Le Polozec, X.; Walker, W.; Reindl, L. RF energy harvesting design using high Q resonators. In Proceedings of the 2009 IEEE MTT-S International Microwave Workshop on Wireless Sensing, Local Positioning, and RFID, Cavtat, Croatia, 24–25 September 2009; pp. 1–4.
205. Saeed, W.; Shoaib, N.; Cheema, H.M.; Khan, M.U. RF energy harvesting for ubiquitous, zero power wireless sensors. *Int. J. Antennas Propag.* **2018**, *2018*, 8903139. [[CrossRef](#)]
206. Muhammad, S.; Jiat Tiang, J.; Kin Wong, S.; Iqbal, A.; Amor, S.; Mohamed Karim, A. A Compact Dual-Port Multi-Band Rectifier Circuit for RF Energy Harvesting. *Comput. Mater. Contin.* **2021**, *68*, 167–184. [[CrossRef](#)]

207. Ajmal, T.; Dyo, V.; Allen, B.; Jazani, D.; Ivanov, I. Design and optimisation of compact RF energy harvesting device for smart applications. *Electron. Lett.* **2014**, *50*, 111–113. [[CrossRef](#)]
208. Ali, M.; Yang, G.; Dougal, R. Miniature circularly polarized rectenna with reduced out-of-band harmonics. *IEEE Antennas Wirel. Propag. Lett.* **2006**, *5*, 107–110. [[CrossRef](#)]
209. Suh, Y.H.; Chang, K. A high-efficiency dual-frequency rectenna for 2.45-and 5.8-GHz wireless power transmission. *IEEE Trans. Microw. Theory Tech.* **2002**, *50*, 1784–1789. [[CrossRef](#)]
210. Suh, Y.H.; Wang, C.; Chang, K. Circularly polarised truncated-corner square patch microstrip rectenna for wireless power transmission. *Electron. Lett.* **2000**, *36*, 600–602. [[CrossRef](#)]
211. Ren, Y.J.; Chang, K. 5.8-GHz circularly polarized dual-diode rectenna and rectenna array for microwave power transmission. *IEEE Trans. Microw. Theory Tech.* **2006**, *54*, 1495–1502.
212. Niotaki, K.; Georgiadis, A.; Collado, A.; Vardakas, J.S. Dual-band resistance compression networks for improved rectifier performance. *IEEE Trans. Microw. Theory Tech.* **2014**, *62*, 3512–3521. [[CrossRef](#)]
213. Bhatt, K.; Kumar, S.; Kumar, P.; Tripathi, C.C. Highly efficient 2.4 and 5.8 GHz dual-band rectenna for energy harvesting applications. *IEEE Antennas Wirel. Propag. Lett.* **2019**, *18*, 2637–2641. [[CrossRef](#)]
214. Nagaveni, S.; Kaddi, P.; Khandekar, A.; Dutta, A. Resistance compression dual-band differential CMOS RF energy harvester under modulated signal excitation. *IEEE Trans. Circuits Syst. I Regul. Pap.* **2020**, *67*, 4053–4062. [[CrossRef](#)]
215. Colaiuda, D.; Ulisse, I.; Ferri, G. Rectifiers' Design and Optimization for a Dual-Channel RF Energy Harvester. *J. Low Power Electron. Appl.* **2020**, *10*, 11. [[CrossRef](#)]
216. Agrawal, S.; Parihar, M.S.; Kondekar, P. A dual-band RF energy harvesting circuit using 4th order dual-band matching network. *Cogent Eng.* **2017**, *4*, 1332705. [[CrossRef](#)]
217. Abdallah, M.; Costantine, J.; Ramadan, A.H.; Tawk, Y. Enhanced radio frequency rectifier with a power splitting/combining topology for wireless energy transfer and harvesting. *IET Microwaves Antennas Propag.* **2019**, *13*, 1280–1286. [[CrossRef](#)]
218. Huang, F.J.; Yo, T.C.; Lee, C.M.; Luo, C.H. Design of circular polarization antenna with harmonic suppression for rectenna application. *IEEE Antennas Wirel. Propag. Lett.* **2012**, *11*, 592–595. [[CrossRef](#)]
219. Li, P.; Long, Z.; Yang, Z. RF Energy Harvesting for Battery-Less and Maintenance-Free Condition Monitoring of Railway Tracks. *IEEE Internet Things J.* **2020**, *8*, 3512–3523. [[CrossRef](#)]
220. Palazzi, V.; Kalialakis, C.; Alimenti, F.; Mezzanotte, P.; Roselli, L.; Collado, A.; Georgiadis, A. Design of a ultra-compact low-power rectenna in paper substrate for energy harvesting in the Wi-Fi band. In Proceedings of the 2016 IEEE Wireless Power Transfer Conference (WPTC), Aveiro, Portugal, 5–6 May 2016; pp. 1–4.
221. Shariati, N.; Rowe, W.S.; Scott, J.R.; Ghorbani, K. Multi-service highly sensitive rectifier for enhanced RF energy scavenging. *Sci. Rep.* **2015**, *5*, 9655. [[CrossRef](#)] [[PubMed](#)]
222. Shen, S.; Zhang, Y.; Chiu, C.Y.; Murch, R.D. A Triple-band High-Gain Multibeam Ambient RF Energy Harvesting System Utilizing Hybrid Combining. *IEEE Trans. Ind. Electron.* **2019**, *67*, 9215–9226. [[CrossRef](#)]
223. Hsu, C.Y.; Lin, S.C.; Tsai, Z.M. Quadband rectifier using resonant matching networks for enhanced harvesting capability. *IEEE Microw. Wirel. Components Lett.* **2017**, *27*, 669–671. [[CrossRef](#)]
224. Liu, J.; Zhang, X.Y. Compact triple-band rectifier for ambient RF energy harvesting application. *IEEE Access* **2018**, *6*, 19018–19024. [[CrossRef](#)]
225. Lu, J.J.; Yang, X.X.; Mei, H.; Tan, C. A four-band rectifier with adaptive power for electromagnetic energy harvesting. *IEEE Microw. Wirel. Components Lett.* **2016**, *26*, 819–821. [[CrossRef](#)]
226. Zeng, M.; Li, Z.; Andrenko, A.S.; Liu, X.; Tan, H.Z. Differential voltage octuple rectifiers for wireless energy harvesting. *Microw. Opt. Technol. Lett.* **2017**, *59*, 1574–1578. [[CrossRef](#)]
227. Khalid, F.; Saeed, W.; Shoaib, N.; Khan, M.U.; Cheema, H.M. Quad-band 3D rectenna array for ambient RF energy harvesting. *Int. J. Antennas Propag.* **2020**, *2020*, 7169846. [[CrossRef](#)]
228. Song, C.; Huang, Y.; Carter, P.; Zhou, J.; Yuan, S.; Xu, Q.; Kod, M. A novel six-band dual CP rectenna using improved impedance matching technique for ambient RF energy harvesting. *IEEE Trans. Antennas Propag.* **2016**, *64*, 3160–3171. [[CrossRef](#)]
229. Singh, N.; Kanaujia, B.K.; Beg, M.T.; Mainuddin; Khan, T.; Kumar, S.; A dual polarized multiband rectenna for RF energy harvesting. *AEU-Int. J. Electron. Commun.* **2018**, *93*, 123–131. [[CrossRef](#)]
230. Tafekirt, H.; Pelegri-Sebastia, J.; Bouajaj, A.; Reda, B.M. A sensitive triple-band rectifier for energy harvesting applications. *IEEE Access* **2020**, *8*, 73659–73664. [[CrossRef](#)]
231. Yoo, T.; Chang, K. 35 GHz integrated circuit rectifying antenna with 33% efficiency. *Electron. Lett.* **1991**, *27*, 2117. [[CrossRef](#)]
232. Singh, N.; Kanaujia, B.; Beg, M.; Mainuddin.; Kumar, S.; Choi, H.C.; Kim, K.W. Low profile multiband rectenna for efficient energy harvesting at microwave frequencies. *Int. J. Electron.* **2019**, *106*, 2057–2071. [[CrossRef](#)]
233. East, T.W. A self-steering array for the SHARP microwave-powered aircraft. *IEEE Trans. Antennas Propag.* **1992**, *40*, 1565–1567. [[CrossRef](#)]
234. Lin, Q.W.; Zhang, X.Y. Differential rectifier using resistance compression network for improving efficiency over extended input power range. *IEEE Trans. Microw. Theory Tech.* **2016**, *64*, 2943–2954. [[CrossRef](#)]
235. Pham, B.L.; Pham, A.V. Triple bands antenna and high efficiency rectifier design for RF energy harvesting at 900, 1900 and 2400 MHz. In Proceedings of the 2013 IEEE MTT-S International Microwave Symposium Digest (MTT), Seattle, WA, USA, 2–7 June 2013; pp. 1–3.

236. Piñuela, M.; Mitcheson, P.D.; Lucyszyn, S. Ambient RF energy harvesting in urban and semi-urban environments. *IEEE Trans. Microw. Theory Tech.* **2013**, *61*, 2715–2726. [[CrossRef](#)]
237. Olgun, U.; Chen, C.C.; Volakis, J.L. Design of an efficient ambient WiFi energy harvesting system. *IET Microwaves Antennas Propag.* **2012**, *6*, 1200–1206. [[CrossRef](#)]
238. Masotti, D.; Costanzo, A.; Del Prete, M.; Rizzoli, V. Genetic-based design of a tetra-band high-efficiency radio-frequency energy harvesting system. *IET Microwaves Antennas Propag.* **2013**, *7*, 1254–1263. [[CrossRef](#)]
239. Oka, T.; Ogata, T.; Saito, K.; Tanaka, S. Triple-band single-diode microwave rectifier using CRLH transmission line. In Proceedings of the 2014 Asia-Pacific Microwave Conference, Sendai, Japan, 4–7 November 2014; pp. 1013–1015.
240. Singh, N.; Kanaujia, B.K.; Tariq Beg, M.; Mainuddin; Kumar, S. A triple band circularly polarized rectenna for RF energy harvesting. *Electromagnetics* **2019**, *39*, 481–490. [[CrossRef](#)]
241. Kimionis, J.; Collado, A.; Tentzeris, M.M.; Georgiadis, A. Octave and decade printed UWB rectifiers based on nonuniform transmission lines for energy harvesting. *IEEE Trans. Microw. Theory Tech.* **2017**, *65*, 4326–4334. [[CrossRef](#)]
242. Abbasian, S.; Johnson, T. High efficiency GaN HEMT synchronous rectifier with an octave bandwidth for wireless power applications. In Proceedings of the 2016 IEEE MTT-S International Microwave Symposium (IMS), San Francisco, CA, USA, 22–27 May 2016; pp. 1–4.
243. Guo, J.; Zhang, H.; Zhu, X. Theoretical analysis of RF-DC conversion efficiency for class-F rectifiers. *IEEE Trans. Microw. Theory Tech.* **2014**, *62*, 977–985. [[CrossRef](#)]
244. Chandravanshi, S.; Katare, K.K.; Akhtar, M.J. Broadband integrated rectenna using differential rectifier and hybrid coupler. *IET Microwaves Antennas Propag.* **2020**, *14*, 1384–1395. [[CrossRef](#)]
245. Bava, G.; Pisani, U.; Pozzolo, V. ‘Source-pull’ technique at microwave frequencies. *Electron. Lett.* **1984**, *20*, 152–154. [[CrossRef](#)]
246. Nimo, A.; Grgić, D.; Reindl, L.M. Optimization of passive low power wireless electromagnetic energy harvesters. *Sensors* **2012**, *12*, 13636–13663. [[CrossRef](#)] [[PubMed](#)]
247. Luo, Y.; Pu, L.; Wang, G.; Zhao, Y. RF Energy Harvesting Wireless Communications: RF Environment, Device Hardware and Practical Issues. *Sensors* **2019**, *19*, 3010. [[CrossRef](#)]
248. Zhang, X.Y.; Du, Z.X.; Xue, Q. High-efficiency broadband rectifier with wide ranges of input power and output load based on branch-line coupler. *IEEE Trans. Circuits Syst. I Regul. Pap.* **2016**, *64*, 731–739. [[CrossRef](#)]
249. Hagerty, J.A.; Helmbrecht, F.B.; McCalpin, W.H.; Zane, R.; Popovic, Z.B. Recycling ambient microwave energy with broad-band rectenna arrays. *IEEE Trans. Microw. Theory Tech.* **2004**, *52*, 1014–1024. [[CrossRef](#)]
250. Song, C.; Huang, Y.; Zhou, J.; Carter, P.; Yuan, S.; Xu, Q.; Fei, Z. Matching network elimination in broadband rectennas for high-efficiency wireless power transfer and energy harvesting. *IEEE Trans. Ind. Electron.* **2016**, *64*, 3950–3961. [[CrossRef](#)]
251. Mansour, M.; Le Polozec, X.; Kanaya, H. Enhanced broadband RF differential rectifier integrated with archimedean spiral antenna for wireless energy harvesting applications. *Sensors* **2019**, *19*, 655. [[CrossRef](#)]
252. Mahfoudi, H.; Tellache, M.; Takhedmit, H. A wideband rectifier array on dual-polarized differential-feed fractal slotted ground antenna for RF energy harvesting. *Int. J. RF Microw. Comput.-Aided Eng.* **2019**, *29*, e21775. [[CrossRef](#)]
253. Singh, N.; Kumar, S.; Kanaujia, B.K.; Beg, M.T.; Mainuddin; Kumar, S.; A compact and efficient graphene FET based RF energy harvester for green communication. *AEU-Int. J. Electron. Commun.* **2020**, *115*, 153059. [[CrossRef](#)]
254. Song, C.; Huang, Y.; Carter, P.; Zhou, J.; Joseph, S.D.; Li, G. Novel compact and broadband frequency-selectable rectennas for a wide input-power and load impedance range. *IEEE Trans. Antennas Propag.* **2018**, *66*, 3306–3316. [[CrossRef](#)]
255. Daskalakis, S.N.; Georgiadis, A.; Goussetis, G.; Tentzeris, M.M. A rectifier circuit insensitive to the angle of incidence of incoming waves based on a Wilkinson power combiner. *IEEE Trans. Microw. Theory Tech.* **2019**, *67*, 3210–3218. [[CrossRef](#)]
256. Wang, Y.Q.; Yang, X.X. Design of a high-efficiency circularly polarized rectenna for 35 GHz microwave power transmission system. In Proceedings of the 2012 Asia-Pacific Power and Energy Engineering Conference, Shanghai, China, 27–29 March 2012; pp. 1–4.
257. Marian, V.; Allard, B.; Vollaie, C.; Verdier, J. Strategy for microwave energy harvesting from ambient field or a feeding source. *IEEE Trans. Power Electron.* **2012**, *27*, 4481–4491. [[CrossRef](#)]
258. Chen, Y.S.; Chiu, C.W. Maximum achievable power conversion efficiency obtained through an optimized rectenna structure for RF energy harvesting. *IEEE Trans. Antennas Propag.* **2017**, *65*, 2305–2317. [[CrossRef](#)]
259. Arrawatia, M.; Baghini, M.S.; Kumar, G. Broadband bent triangular omnidirectional antenna for RF energy harvesting. *IEEE Antennas Wirel. Propag. Lett.* **2015**, *15*, 36–39. [[CrossRef](#)]
260. Kotani, K.; Sasaki, A.; Ito, T. High-efficiency differential-drive CMOS rectifier for UHF RFIDs. *IEEE J. Solid-State Circuits* **2009**, *44*, 3011–3018. [[CrossRef](#)]
261. Kuzle, I.; Pandzic, H.; Bosnjak, D. The true inventor of the radio communications. In Proceedings of the 2008 IEEE History of Telecommunications Conference, Paris, France, 11–12 September 2008; pp. 20–23.
262. Park, J.; Kim, Y.; Yoon, Y.J.; So, J.; Shin, J. Rectifier design using distributed Greinacher voltage multiplier for high frequency wireless power transmission. *J. Electromagn. Eng. Sci.* **2014**, *14*, 25–30. [[CrossRef](#)]
263. Gozel, M.A.; Kahriman, M.; Kasar, O. Design of an efficiency-enhanced Greinacher rectifier operating in the GSM 1800 band by using rat-race coupler for RF energy harvesting applications. *Int. J. RF Microw. Comput.-Aided Eng.* **2019**, *29*, e21621. [[CrossRef](#)]
264. Brown, W.C. The history of power transmission by radio waves. *IEEE Trans. Microw. Theory Tech.* **1984**, *32*, 1230–1242. [[CrossRef](#)]

265. Fan, S.; Yuan, Z.; Gou, W.; Zhao, Y.; Song, C.; Huang, Y.; Zhou, J.; Geng, L. A 2.45-GHz rectifier-booster regulator with impedance matching converters for wireless energy harvesting. *IEEE Trans. Microw. Theory Tech.* **2019**, *67*, 3833–3843. [CrossRef]
266. Han, Y.; Leitermann, O.; Jackson, D.A.; Rivas, J.M.; Perreault, D.J. Resistance compression networks for radio-frequency power conversion. *IEEE Trans. Power Electron.* **2007**, *22*, 41–53. [CrossRef]
267. Barton, T.W.; Gordonson, J.M.; Perreault, D.J. Transmission line resistance compression networks and applications to wireless power transfer. *IEEE J. Emerg. Sel. Top. Power Electron.* **2014**, *3*, 252–260. [CrossRef]
268. Wang, Z.; Zhang, W.; Jin, D.; Xie, H.; Lv, X. A full-wave RF energy harvester based on new configurable diode connected MOSFETs. In Proceedings of the 2016 IEEE International Conference on Microwave and Millimeter Wave Technology (ICMMT), Beijing, China, 5–8 June 2016; Volume 1, pp. 117–119.
269. Sun, H.; Zhong, Z.; Guo, Y.X. An adaptive reconfigurable rectifier for wireless power transmission. *IEEE Microw. Wirel. Components Lett.* **2013**, *23*, 492–494. [CrossRef]
270. Li, C.J.; Lee, T.C. 2.4-GHz high-efficiency adaptive power. *IEEE Trans. Very Large Scale Integr. (VLSI) Syst.* **2013**, *22*, 434–438. [CrossRef]
271. Liu, Z.; Zhong, Z.; Guo, Y.X. Enhanced dual-band ambient RF energy harvesting with ultra-wide power range. *IEEE Microw. Wirel. Components Lett.* **2015**, *25*, 630–632. [CrossRef]
272. Boot, H.A.; Randall, J.T. Historical notes on the cavity magnetron. *IEEE Trans. Electron Devices* **1976**, *23*, 724–729. [CrossRef]
273. Broadcom, L. HSMS-2850 Datasheet PDF. 2014. Available online: <https://www.farnell.com/datasheets/47810.pdf> (accessed on 15 September 2019).
274. Masotti, D.; Costanzo, A.; Francia, P.; Filippi, M.; Romani, A. A load-modulated rectifier for RF micropower harvesting with start-up strategies. *IEEE Trans. Microw. Theory Tech.* **2014**, *62*, 994–1004. [CrossRef]
275. Wong, S.W.; Sun, G.H.; Zhu, L.; Chen, Z.N.; Chu, Q.X. Integration of Wireless Coil and Bluetooth Antenna for High Charging and Radiation Efficiencies. *IEEE Trans. Components Packag. Manuf. Technol.* **2018**, *8*, 1292–1299. [CrossRef]
276. Bernard, W.C. *Tesla: Inventor of the Electrical Age*; Princeton University Press: Princeton, NJ, USA, 2015.
277. Nimo, A.; Beckedahl, T.; Ostertag, T.; Reindl, L. Analysis of passive RF-DC power rectification and harvesting wireless RF energy for micro-watt sensors. *AIMS Energy* **2015**, *3*, 184–200. [CrossRef]
278. Strassner, B.; Chang, K. Microwave power transmission: Historical milestones and system components. *Proc. IEEE* **2013**, *101*, 1379–1396. [CrossRef]
279. Eltresy, N.; Eiseakh, D.; Abdallah, E.; Elhenawy, H. RF energy harvesting using efficiency dual band rectifier. In Proceedings of the 2018 Asia-Pacific Microwave Conference (APMC), Kyoto, Japan, 6–9 November 2018; pp. 1453–1455.
280. Mouapi, A.; Hakem, N. A selective rectifier for RF energy harvesting for IoT applications. In Proceedings of the 2018 IEEE International Symposium on Antennas and Propagation & USNC/URSI National Radio Science Meeting, Boston, MA, USA, 8–13 July 2018; pp. 2523–2524.
281. Mouapi, A.; Hakem, N.; Kamani, G.V. A selective rectifier for RF energy harvesting under non-stationary propagation conditions. In Proceedings of the 2018 IEEE International Conference on Environment and Electrical Engineering and 2018 IEEE Industrial and Commercial Power Systems Europe (EEEIC/I&CPS Europe), Palermo, Italy, 12–15 June 2018; pp. 1–6.
282. Yo, T.C.; Lee, C.M.; Hsu, C.M.; Luo, C.H. Compact circularly polarized rectenna with unbalanced circular slots. *IEEE Trans. Antennas Propag.* **2008**, *56*, 882–886. [CrossRef]
283. Georgiadis, A.; Andia, G.V.; Collado, A. Rectenna design and optimization using reciprocity theory and harmonic balance analysis for electromagnetic (EM) energy harvesting. *IEEE Antennas Wirel. Propag. Lett.* **2010**, *9*, 444–446. [CrossRef]
284. Olgun, U.; Chen, C.C.; Volakis, J.L. Investigation of rectenna array configurations for enhanced RF power harvesting. *IEEE Antennas Wirel. Propag. Lett.* **2011**, *10*, 262–265. [CrossRef]
285. Takhedmit, H.; Cirio, L.; Bellal, S.; Delcroix, D.; Picon, O. Compact and efficient 2.45 GHz circularly polarised shorted ring-slot rectenna. *Electron. Lett.* **2012**, *48*, 253–254. [CrossRef]
286. Strassner, B.; Chang, K. Highly efficient C-band circularly polarized rectifying antenna array for wireless microwave power transmission. *IEEE Trans. Antennas Propag.* **2003**, *51*, 1347–1356. [CrossRef]
287. Mavaddat, A.; Armaki, S.H.M.; Erfanian, A.R. Millimeter-Wave Energy Harvesting Using  $4 \times 4$  Microstrip Patch Antenna Array. *IEEE Antennas Wirel. Propag. Lett.* **2014**, *14*, 515–518. [CrossRef]
288. Lorenz, C.H.; Hemour, S.; Liu, W.; Badel, A.; Formosa, F.; Wu, K. Hybrid power harvesting for increased power conversion efficiency. *IEEE Microw. Wirel. Components Lett.* **2015**, *25*, 687–689. [CrossRef]
289. Gu, X.; Hemour, S.; Guo, L.; Wu, K. Integrated cooperative ambient power harvester collecting ubiquitous radio frequency and kinetic energy. *IEEE Trans. Microw. Theory Tech.* **2018**, *66*, 4178–4190. [CrossRef]
290. Nintanavongsa, P.; Muncuk, U.; Lewis, D.R.; Chowdhury, K.R. Design optimization and implementation for RF energy harvesting circuits. *IEEE J. Emerg. Sel. Top. Circuits Syst.* **2012**, *2*, 24–33. [CrossRef]
291. Yoon, I.J.; Kim, H.; Yoon, H.; Yoon, Y.; Kim, Y.H. Ultra-wideband tapered slot antenna with band cutoff characteristic. *Electron. Lett.* **2005**, *41*, 629–630. [CrossRef]
292. Hemour, S.; Wu, K. Radio-frequency rectifier for electromagnetic energy harvesting: Development path and future outlook. *Proc. IEEE* **2014**, *102*, 1667–1691. [CrossRef]
293. Masuch, J.; Delgado-Restituto, M.; Milosevic, D.; Baltus, P. Co-integration of an RF energy harvester into a 2.4 GHz transceiver. *IEEE J. Solid-State Circuits* **2013**, *48*, 1565–1574. [CrossRef]

294. Scott, H.H. A new type of selective circuit and some applications. *Proc. Inst. Radio Eng.* **1938**, *26*, 226–235. [[CrossRef](#)]
295. Reddy, V.; Sarma, N. Compact circularly polarized asymmetrical fractal boundary microstrip antenna for wireless applications. *IEEE Antennas Wirel. Propag. Lett.* **2014**, *13*, 118–121. [[CrossRef](#)]
296. Papotto, G.; Carrara, F.; Palmisano, G. A 90-nm CMOS threshold-compensated RF energy harvester. *IEEE J. Solid-State Circuits* **2011**, *46*, 1985–1997. [[CrossRef](#)]
297. Shadmehr, H.; Grimaccia, F.; Gruosso, G.; Mussetta, M.; Zich, R. Optimized Antenna for Low UHF Range Wireless Power Transfer. 2013. Available online: <https://www.praiseworthyprize.org/jsm/index.php?journal=irecap&page=article&op=view&path%5B%5D=10683> (accessed on 5 March 2020).
298. Dolgov, A.; Zane, R.; Popovic, Z. Power management system for online low power RF energy harvesting optimization. *IEEE Trans. Circuits Syst. I Regul. Pap.* **2010**, *57*, 1802–1811. [[CrossRef](#)]